JGR Solid Earth

RESEARCH ARTICLE
10.1029/2022JB025269

Key Points:
- The first comprehensive rock magnetism study is performed for both splash-form and Muong Nong-type tektites from South China
- Samples from China generally exhibit lower magnetic susceptibility, natural remanent magnetization, and ratio of equivalent magnetization
- Different shock levels and cooling histories of tektite melt can explain the observed magnetic properties, and Fe-S spherules are found

Supporting Information:
Supporting Information may be found in the online version of this article.

Correspondence to:
Z. Xiao,
xiaozhiyong@mail.sysu.edu.cn

Citation:
Pan, Q., Xiao, Z., Wu, Y., Shi, T., Yin, Z., Yan, P., & Li, Y. (2023). Magnetic properties of Australasian tektites from South China. *Journal of Geophysical Research: Solid Earth*, *128*, e2022JB025269. https://doi.org/10.1029/2022JB025269

Received 27 JUL 2022
Accepted 5 MAR 2023

Author Contributions:
Conceptualization: Zhiyong Xiao
Data curation: Qing Pan, Zhiyong Xiao, Yunhua Wu, Taiheng Shi, Zongjun Yin, Pan Yan, Ye Li
Formal analysis: Qing Pan, Zhiyong Xiao, Yunhua Wu, Zongjun Yin, Pan Yan, Ye Li
Funding acquisition: Zhiyong Xiao
Investigation: Qing Pan, Zhiyong Xiao
Methodology: Qing Pan, Zhiyong Xiao, Yunhua Wu, Zongjun Yin
Project Administration: Zhiyong Xiao
Resources: Zhiyong Xiao
Software: Qing Pan
Supervision: Zhiyong Xiao
Writing – original draft: Qing Pan
Writing – review & editing: Qing Pan, Zhiyong Xiao

Magnetic Properties of Australasian Tektites From South China

Qing Pan[1], Zhiyong Xiao[1,2], Yunhua Wu[1], Taiheng Shi[3], Zongjun Yin[4], Pan Yan[1], and Ye Li[2,5]

[1]Planetary Environmental and Astrobiological Research Laboratory, School of Atmospheric Sciences, Sun Yat-Sen University, Zhuhai, China, [2]Center for Excellence in Comparative Planetology, Chinese Academy of Science, Hefei, China, [3]School of Earth Sciences, Hubei Key Laboratory of Critical Zone Evolution, China University of Geosciences (Wuhan), Wuhan, China, [4]State Key Laboratory of Palaeobiology and Stratigraphy, Nanjing Institute of Geology and Paleontology, Center for Excellence in Life and Paleoenvironment, Chinese Academy of Sciences, Nanjing, China, [5]Key Laboratory of Planetary Sciences, Purple Mountain Observatory, Chinese Academy of Sciences, Nanjing, China

Abstract South China, the northern part of the Australasian strewn field (AASF) of tektites and microtektites is located at the uprange of the hypothesized source crater that is still unconfirmed. Magnetic properties of impact glasses are an important indicator of their source materials and thermal history. Extensive magnetic investigations have been performed on various AASF tektites sampled from both the Indochina Peninsula and further south, but such information remains sparse for those sampled from South China. Here, we present a detailed rock magnetism study for both Muong Nong-type and splash-form AASF tektites from South China, showing that all the tektites have rather weak remanent magnetization, but ferromagnetic information can be extracted from their dominating paramagnetic signal. Signals caused by superparamagnetic particles are elusive, but those of single domain magnetite are detected in the splash-form tektites, and signals of pseudo-single domain magnetite are discovered in the Muong Nong-type tektites. Each morphological type of tektites from a same geographic area exhibits large dispersions in their magnetic properties. Across the entire AASF, the Muong Nong-type tektites from South China exhibit the lowest average magnetic susceptibility, and the splash-form tektites exhibit the smallest average natural remanent magnetization and ratio of equivalent magnetization. The observed heterogeneous magnetic properties are mainly caused by the different contents and sizes of magnetic particles, which can be explained by the different shock level and/or cooling history of the tektite melts. Micro-sized immiscible Fe-S spherules in the Muong Nong-type tektites from South China were likely originated from the pre-impact target.

Plain Language Summary About 0.78 million years ago, an about 1 km diameter asteroid or comet ended its trajectory on Earth. Instantaneously, massive continental sediments were molten and ejected, and natural glasses (tektites) were quenched and deposited across vast areas over 1×10^8 km^2, forming the largest known Cenozoic strewn field of tektites and microtektites, the Australasian strewn field (AASF). The impact site is still unconfirmed. Magnetic properties of impact glasses are indicative to their source materials and thermal history. This study presents the first rock magnetic measurements for AASF tektites from South China. We find that while the samples are dominated by paramagnetic signals, signals caused by single domain magnetite are detected, and the Muong Nong-type tektites contain pseudo-single domain magnetite. Signals of superparamagnetic grains are elusive. With heterogeneous magnetic properties, tektites from South China generally exhibit lower magnetic susceptibility, natural remanent magnetization, and ratios of equivalent magnetization than the rest of AASF. The observed magnetic properties can be explained by different shock levels and cooling histories of the tektite melts, but strong magnetic field(s) recorded by some Muong Nong-type tektites have an unknown origin. The first occurrence of Fe-S spherules in tektites from South China might originate from target materials.

1. Introduction and Background

Tektites are natural glasses quenched from molten terrestrial surface materials during meteoritic impact events (e.g., Glass & Simonson, 2013; Koeberl, 1986; Schwarcz, 1962; Taylor, 1962). After being ejected from the impact site, rapid cooling and solidification of the precursor impact melt of tektites were mostly completed during flight (Baldwin et al., 2015; Elkins-tanton et al., 2003). The specific geographic area where tektites were landed is

10.1029/2022JB025269

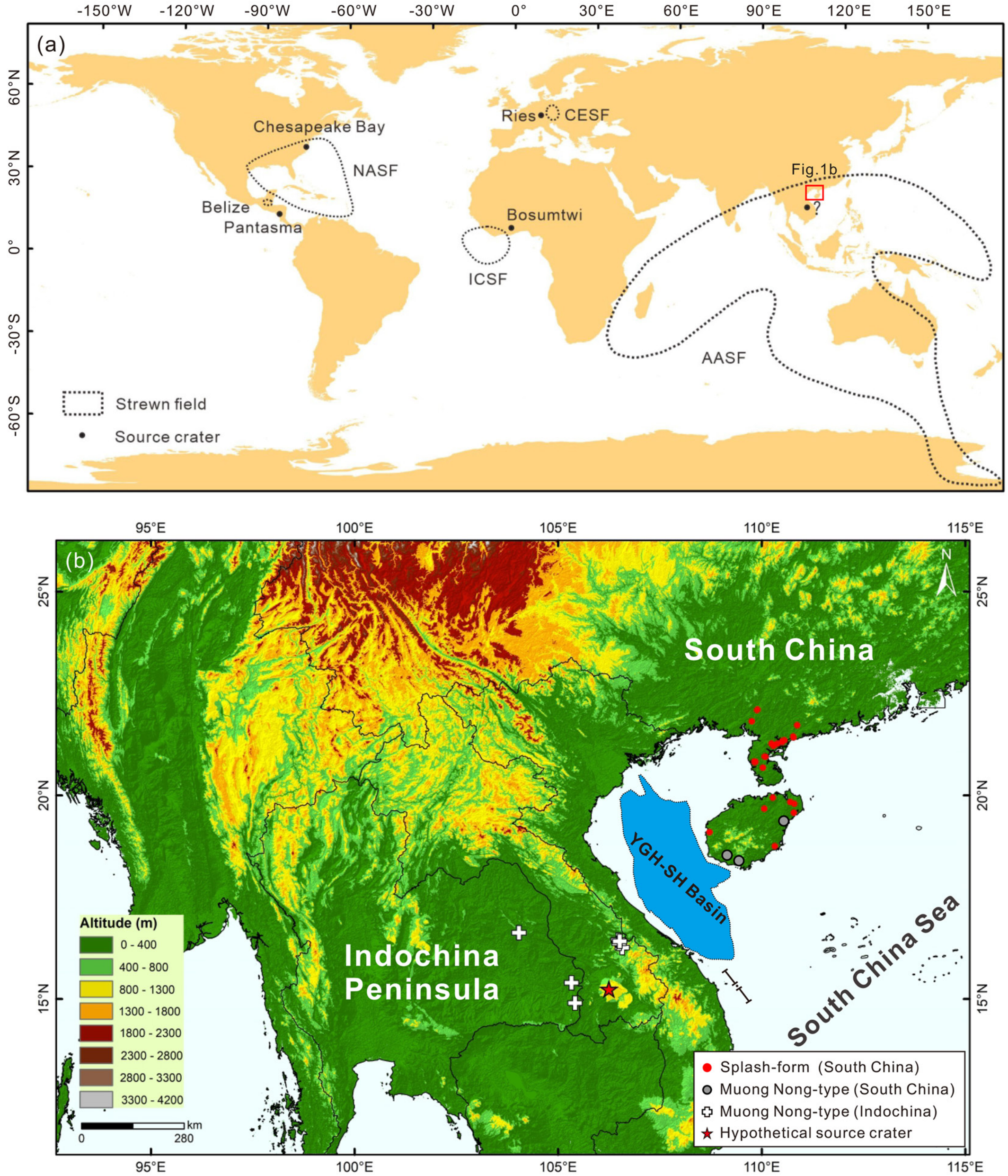

Figure 1. Distribution of Australasian tektites at South China investigated in this study. The source crater of AASF is not confirmed, and the position of potential source crater (black dot in panel (a) and red star in panel (b)) was referred from Sieh et al. (2020). (a) Approximated geographic boundaries and source craters of the five major Cenozoic strewn fields of tektites and microtektites on Earth. AASF = Australasian strewn field, NASF = North American strewn field, CESF = Central European strewn field, ICSF = Ivory Coast strewn field, YGH-SH Basin = Yinggehai-Song Hong Basin. Red box denotes boundaries for the region in panel (b). Locations where tektites and microtektites were discovered are not annotated in this map. (b) Map of South China and Indochina Peninsula. Red circles represent locations of splash-form tektites and gray circles are locations of Muong Nong-type tektites investigated in this study. White crosses represent the locations of Muong Nong-type indochinites that have published magnetic data (de Gasparis et al., 1975; Gattacceca et al., 2021).

called a strewn field (Chapman, 1971; Glass, 1990). So far, five major Cenozoic strewn fields are recognized on Earth (Figure 1a), including the Australasian strewn field (AASF), North American strewn field (NASF), Central European strewn field (CESF), Ivory Coast strewn field (ICSF), and the recently confirmed Belize strewn field (Koeberl et al., 2022; Rochette et al., 2021). The source craters of NASF, CESF, ICSF and Belize strewn field have been identified, but that of AASF, the largest one that covers about 20% of the Earth's surface (Figure 1a), is still not confirmed after more than half a century survey.

AASF was formed at 788.1 ± 3 ka ago (Jourdan et al., 2019), and its highly-asymmetry geographic boundary (Figure 1a) indicates an oblique impact from north–northwest to south–southeast (Artemieva, 2008b). AASF may contain about 10^8 tons of tektites and microtektites (Glass, 1990), and the source impactor may be about 1 km in diameter (Artemieva, 2013; Goderis et al., 2017). The parent crater of AASF has an estimated diameter of over 30 km and depth of over several kilometers (Glass & Koeberl, 2006; Glass & Pizzuto, 1994; Prasad et al., 2007). This exceptionally young impact event was postulated to have caused immediate regional environmental changes at the early-middle Pleistocene transition, which probably reduced the population of *Homo erectus* that once lived in the Southeast Asia and South China (Glass & Heezen, 1967; Haines et al., 2004; Hyodo et al., 2011; Li et al., 2021). While the topography of the parent crater, if formed on land, should not have been entirely removed by erosion, deflation and/or deposition, extensive search via remote sensing and field investigations yields no confirmed case yet at the continent (Kenkmann et al., 2014; Melosh, 2020; Mizera, 2022; Mizera et al., 2016; Sieh et al., 2020). The geochemistry of tektites, such as ^{10}Be concentrations, Rb-Sr ratio in tektites, and Na, K contents in microtektites (Blum et al., 1992; Folco, Glass, et al., 2010; Goderis et al., 2017; Ma et al., 2004; Rochette et al., 2018), shows distribution patterns that converge toward the central to northern part of the Indochina Peninsula and the adjacent offshore regions. Similar distribution patterns were noticed in the spatial density of various forms of AASF microtektites (e.g., those in deep ocean sediments; Lee & Wei, 2000; Glass & Pizzuto, 1994) and other shocked materials (e.g., remanent shocked mineral fragments in tektites; Folco, Perchiazzi, et al., 2010; Cavosie et al., 2018). Therefore, it has been hypothesized that the source crater might be located in the floor of the South China Sea (Chaussidon & Koeberl, 1995; Schnetzler et al., 1988), possibly in the center to southern part of the Gulf of Tonkin or the Yinggehai-Song Hong Basin (Ma et al., 2004; Whymark, 2018, 2021).

Four major types of tektites are recognized in AASF: (a) Muong Nong-type tektites that have irregular and blocky shapes and layering structures; (b) splash-form tektites that typically exhibit rotational shapes, such as spheres, disks, teardrops, and dumbbells, and their irregular-shaped fragments are usually encountered in the field; (c) ablated splash-form tektites that typically occur as flanged buttons surrounded by ablation rims, and they were formed by re-melting of the anterior during hypervelocity return to the Earth's atmosphere; (d) microtektites that are less than 1 mm in sizes and mostly found in deep ocean sediments and recently found at Antarctic (Folco, Glass, et al., 2010). While it is generally agreed that AASF was formed by an asteroidal impact on thick silt-sized homogeneous sedimentary materials (Ackerman et al., 2020; Chaussidon & Koeberl, 1995; Glass & Barlow, 1979; Ma et al., 2004), it has also been proposed but questioned that mafic igneous rocks might be part of the target materials (Mizera, 2022; Sieh et al., 2020). Some AASF tektites that contain relatively high contents of calcium may indicate heterogeneous distribution of carbonates in the pre-impact target (Amare & Koeberl, 2006). Besides uncertainties about the lithology of the target materials, impactor components in AASF tektites and microtektites are also obscure due to low and nonuniform contents of extraterrestrial components (Chao et al., 1962, 1964; Goderis et al., 2017; Koeberl, 1994).

1.1. AASF Tektites at South China

AASF tektites were also found at South China such as the Guangdong, Guangxi and Hainan Provinces. They were recognized based on geochemical and morphological investigations in the 1960s (Barnes, 1969; Li, 1963). Their fission track ages (Yan et al., 1979; Zhang et al., 1991), isotopic ages (Hou et al., 2000; Jourdan et al., 2019), and major and trace element concentrations are consistent with those of AASF tektites at other places, indicating that the tektites were formed by a same impact event in a relatively homogeneous target (Ho & Chen, 1996; Lee et al., 2004; Lin et al., 2011). Especially, Muong Nong-type tektites that are as large as about 10 kg (Futrell & Wasson, 1993; Yuan, 1981) were discovered at Hainan (Figure 1b), which is located at more than 500 km to the northeast of the layered tektites zone at the Indochina Peninsula (Fiske et al., 1999).

South China is an important geographic branch of AASF (Figure 1b), because this area is the northern portion of this strewn field (Yan et al., 2022), and it corresponds to the uprange of the hypothesized impactor trajectory. Numerical simulations suggested that impact plume formed by an oblique impact would be inclined toward the downrange, so that much fewer impact melt that was engulfed in the impact plume was capable to form tektites at the uprange (Artemieva, 2013; Stöffler et al., 2002). Therefore, compared to most other Cenozoic tektites, AASF tektites at South China are unique in terms of locations, since they are located at the uprange and close to the hypothesized source crater (Ma et al., 2004; Whymark, 2021). Compared with AASF tektites that are located at the other ejection azimuths with respect to a hypothesized source crater, tektites at South China may contain unique information about the impact history and possible location of the source crater.

1.2. Magnetic Properties of AASF Tektites

Rock magnetism is an important method to identify natural glasses of different origins (Rochette et al., 2022), and it has been extensively used to investigate the thermal history, source materials, and parent crater of various impact glasses, especially tektites. For example, Senftle et al. (2000) distinguished Belize tektites from those of the other four major Cenozoic strewn fields based on the much higher magnetic susceptibilities of belizites (average 121×10^{-9} m^3/kg), which are closer to those of the other impact glasses formed by the Pantasma crater (Rochette et al., 2019). Pantasma has recently been confirmed as the source crater of the Belize strewn field (Rochette et al., 2021). Paleomagnetic study for basaltic impact glasses formed by the Lonar crater (1.88 km diameter; India) revealed that small (<0.5 g) splash-form samples exhibit unstable and weak natural remanent magnetization (NRM), interpreted to be caused by motional magnetization during cooling in flight (Weiss et al., 2010). On the contrary, larger (>0.8 g) and irregular-shaped non-splash-form impact glasses formed by Lonar have stable NRM that are about 10^2–10^3 larger than those of small glasses, suggesting that the larger ones were cooled through their Curie points (e.g., magnetite, 585°C) after landing (Weiss et al., 2010). The widespread and multiple types of AASF tektites would be extremely valuable materials for rock magnetic and paleomagnetic studies to reveal their thermal history, precursor material, and potential parent crater.

Early studies revealed uniform magnetic susceptibilities of AASF tektites at different locations (Donofrio, 1977; Senftle & Thorpe, 1959; Thorpe et al., 1963; Werner & Borradaile, 1998). This phenomenon was interpreted to be caused by an extreme homogenization process during the impact process, and the target material may be single-lithology modern marine deposits (Werner & Borradaile, 1998). Senftle and Thorpe (1959) performed a pioneering magnetic study for different Cenozoic tektites and revealed that the magnetic susceptibility of AASF tektites in the Java island (i.e., javanites), Billiton island (i.e., billitonites), and the Philippines (i.e., philippinites) was comparable, suggesting that their precursor materials may be similar in composition. For comparison, moldavites of CESF exhibit lower magnetic susceptibility, indicating that tektites from different strewn fields may have different susceptibilities (Senftle & Thorpe, 1959). In term of geochemistry, each Cenozoic strewn field of tektites and microtektites has a distinctive composition zone (e.g., FeO content) that can be differentiated from the other strewn field (Glass, 1990; Koeberl, 1986). A positive correlation between the average FeO content and magnetic susceptibility of Cenozoic tektites was once noticed, suggesting that magnetic materials inherited from the precursor target materials may significantly affect the magnetic properties of tektites (Rochette et al., 2015; Senftle & Thorpe, 1959). On the contrary, recent measurements of magnetic susceptibility for hundreds of tektites from different areas of AASF (including tektites from the Guangdong Province) revealed substantial differences (Rochette et al., 2019). Heterogeneous contamination by ferromagnetic materials from local soils to the samples and/or different contents of magnetic elements (e.g., Fe, Mn, Cr) in the tektites was invoked to explain this observation (Rochette et al., 2019). On the other hand, it is well constrained that AASF tektites at different geographic areas exhibit systematic variations in the geochemistry, and different compositional groups of tektites may occur in a same area (Amare & Koeberl, 2006; Chapman & Scheiber, 1969; Glass & Koeberl, 2006; Koeberl, 1992; Lin et al., 2011; Westgate et al., 2021). For example, most australites (i.e., AASF tektites from Australia) belong to the high-Na/K group, and they have higher contents of FeO and ferromagnetic elements (e.g., Ni, Co) than indochinites (i.e., the AASF tektites from Indochina Peninsula), indicating that australites may have incorporated more residual iron oxides from the pre-impact target materials and/or meteoritic components (Amare & Koeberl, 2006; Goderis et al., 2017; Werner & Borradaile, 1998). Therefore, the magnetic susceptibility of AASF tektites from South China is an important information to evaluate chemical homogeneities of the precursor materials.

Rock magnetism also provides important information on the thermal history of AASF tektites. Donofrio (1977) acquired laboratory thermal remanent magnetization (TRM) in a 40 μT ambient field for cores of splash-form philippinites and ablated splash-form australites (0.09–0.38×10^{-6} Am^2/kg). The TRM of the samples was comparable with their NRM before heating (0.09–0.25×10^{-6} Am^2/kg), leading to an interpretation that both types of AASF tektites were solidified in the geomagnetic field. de Gasparis et al. (1975) investigated the paleomagnetic properties of Muong Nong-type tektites from the southern Laos and northeastern Thailand, suggesting that some fine grains of iron-rich titanomagnetite may carry a stable NRM that was acquired during cooling in the ambient geomagnetic field. Gattacceca et al. (2021) updated the paleomagnetic data for Muong Nong-type tektites

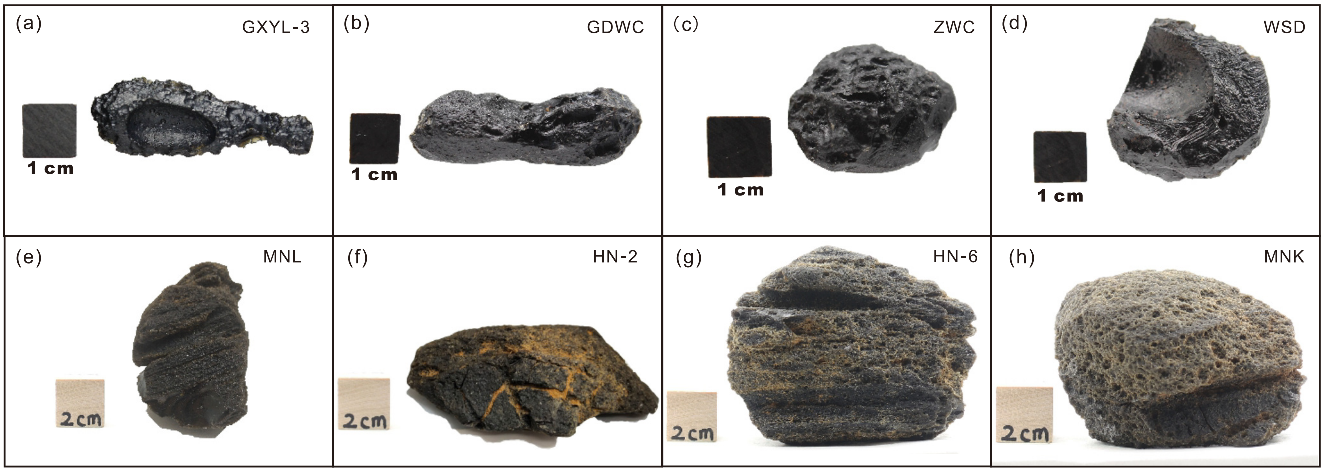

Figure 2. Typical AASF tektites from South China that were investigated in this study. (a–d) Typical splash-form tektites with teardrop, rods and sphere shapes, and their fragments. (e–h) Muong Nong-type tektites from the Hainan Province.

from the southern Laos and northeastern Thailand, revealing that their paleomagnetic inclinations with respect to the layering plane were clustered around an average value of 18 ± 12°, close to the local paleolatitude at ~0.78 Ma. This observation was interpreted as evidence supporting that the Muong Nong-type tektites may cool from puddles of impact melt on the ground (Gattacceca et al., 2021), in which horizontal shearing may occur in the interior (Barnes and Pitakpaivan, 1962; de Gasparis et al., 1975). Alternatively, it has long being argued that Muong Nong-type tektites should have been completely solidified in terms of mechanical properties during flight, and the layering structures may be formed during cooling in flight (Fiske et al., 1996; Tada et al., 2020). Detailed rock magnetism study for Muong Nong-type tektites from different regions of AASF would provide additional insights about their cooling history, especially for those located at the uprange in South China.

Up to now, magnetic investigations for AASF tektites from South China are sparse, and systematic studies of magnetic inclusions in these tektites are lacking. In this study, we present detailed rock magnetic measurements and petrographic observations for magnetic particles in AASF tektites that were sampled from South China. Our targets are to (a) compare the magnetic properties of AASF tektites that were deposited at various azimuths and distances with respect to the interpreted impactor trajectory and potential source crater at Indochina; (b) decode thermal histories of tektites recorded in their magnetic properties; and (c) locate possible magnetic particles in the tektites and investigate their implications to the precursor materials.

2. Materials and Methods

2.1. Samples

Our field investigations at South China (2016–2018) yielded over 1,000 pieces of tektites from Guangdong, Guangxi and Hainan Provinces at South China. AASF tektites in these areas typically occur within the Beihai Formation (Yuan, 1981; Zhang et al., 1991), which is composed of the Middle-Pleistocene lithified fluvial deposits (Zhu et al., 2001, 2006). Our field investigation focused on outcrops of the Beihai Formation where AASF tektites were discovered before. Figure S1 in Supporting Information S1 shows a photo for the stratigraphic occurrence of the tektites.

The collected tektites are dominated by irregular-shaped fragments of splash-form tektites, and large ones exhibit spherical and other rotational forms such as dumbbell, rod and teardrops (Figure 2). Muong Nong-type tektites that are as large as about 12 cm in lengths (up to ~500 g) were also collected from the Hainan Province (Figure 2). Table S1 shows the information of samples used in this study, including their IDs, locations, and morphological types.

2.2. X-Ray Fluorescence Analyses

Besides the field evidence from stratigraphic occurrences (Figure S1 in Supporting Information S1), our collected samples are confirmed as AASF tektites based on their compositional comparisons with the four major

Table 1
Contents of Major Elements for Eight Random Tektite Samples From South China

Sample name	SiO_2	TiO_2	Al_2O_3	Fe_2O_3	MnO	MgO	CaO	Na_2O	K_2O	LOI	Total
GDMM	74.04	0.66	11.60	4.31	0.07	1.78	1.24	1.24	2.22	2.63	99.82
GDWC	71.11	0.76	12.67	4.83	0.07	2.06	1.44	1.41	2.26	3.11	99.76
GDZJ	71.93	0.71	12.66	4.63	0.07	1.76	1.13	1.21	2.24	3.13	99.49
GDLZ	72.61	0.73	11.85	4.79	0.07	1.83	1.32	1.38	2.40	3.23	100.30
GDXW	72.52	0.68	12.03	4.52	0.07	1.76	1.26	1.45	2.38	3.20	99.91
HNHK	74.82	0.73	10.79	4.36	0.06	1.65	1.01	1.37	2.11	3.23	100.15
HNWC	72.83	0.71	11.81	4.54	0.07	1.74	1.23	1.53	2.44	2.97	99.93
HNWN	73.63	0.73	11.34	4.53	0.06	1.72	1.10	1.54	2.34	3.28	100.32

Note. The data were obtained by XRF and LOI is the abbreviation for the loss-on-ignition. Unit is weight percent.

Cenozoic strewn fields of tektites. Major-element compositions of eight random samples (Table 1) were acquired using a Shimadzu XRF-1800 spectrometer at the State Key Laboratory of Geological Processes and Mineral Resources, China University of Geosciences (Wuhan). The operation conditions involved a Rh-anode X-ray tube with a voltage of 40 kV and current of 70 mA. 0.5 g of tektite powder and 5 g of compound flux ($Li_2B_4O_7$: $LiBO_2$ = 12:22) were fused in a high-frequency melting furnace for 11 min at ∼1050°C in 95% Pt–5% Au crucibles (Ma et al., 2012). The loss-on-ignition (LOI) was measured on dried rock powder by heating in a pre-heated corundum crucible to 1000°C for 90 min and recording the percentage weight loss (Ma et al., 2012). Calibration curves used for quantification were produced by bivariate regression of data from ∼63 reference materials encompassing a wide range of silicate compositions. Precision is better than 4% and accuracy is better than 3% for major elements (Ma et al., 2012). Table 1 shows the major element compositions derived from the X-ray fluorescence (i.e., XRF) measurements.

2.3. Magnetic Measurements

To eliminate possible contaminations by weathered products that are adhered on surfaces of the tektites, all samples were cut into cubic subsamples using a low-speed diamond wire saw. The cutting was cooled with circulating deionized purified water. We set up a relative orientation for the Muong Nong-type tektites according to their interior layering planes, that is, *z*-axis being perpendicular to the interior layers. Afterward, the glass cubes were washed using an acetate buffer solution, 4:1 (vol/vol) of 2 M acetic acid and 1 M sodium acetate, for 24 hr to remove impurities. The samples were then cleaned in an ultrasonic bath for 20 min before air drying.

To estimate the content of various magnetic materials in the tektite samples, we selected 62 Muong Nong-type and seventy-two splash-form samples to measure their low- (χ_{lf}, 976 Hz) and high- (χ_{hf}, 15,616 Hz) frequency magnetic susceptibility. The MFK1-FA Kappabridge (Agico Ltd., Brno, with sensitivity of 2×10^{-8} SI) at the Environmental Magnetism Laboratory of Guangzhou Institute of Geochemistry, Chinese Academy of Sciences was employed. The frequency-dependent susceptibility ($\chi_{fd}\%$) were defined as a percentage $\chi_{fd}\% = (\chi_{lf} - \chi_{hf})/\chi_{lf} \times 100\%$ (Dearing et al., 1996).

To investigate possible phase transition(s) of potential magnetic minerals in our tektites upon thermal treatment, we selected two Muong Nong-type and two splash-form samples for high-temperature susceptibility measurements using a MFK1-FA Kappabridge equipped with a CS-4 high-temperature furnace (Agico Ltd., Brno). Temperature-dependent susceptibility curves were obtained by cycling samples in an argon atmosphere (the flow rate is 100 ml/min) at a frequency of 976 Hz from room temperature up to 700°C and back to room temperature. The susceptibility of each sample was obtained by subtracting the measured background susceptibility (i.e., furnace tube correction) using the CUREVAL 8.0 program (Agico Ltd., Brno).

To detect and identify possible ferromagnetic signals in the tektites, we selected twenty Muong Nong-type and thirty-one splash-form samples for hysteresis parameters analyses. The hysteresis parameters of Muong Nong-type samples were measured using a vibrating sample magnetometer (MicroMag VSM 3900, with sensitivity of 10^{-10} Am^2 and a maximum applied field of 1 T) at the Magnetics Laboratory of Sun Yat-Sen University.

Considering that the splash-form tektites have weak NRM intensity ($\leq 10^{-7}$Am^2/kg; measured in this study), we prepared parallel pieces for the same samples and repeated the measurements using a higher sensitivity vibrating sample magnetometer (VSM 8604, with sensitivity of 10^{-12} Am^2; maximum applied field of 1 T) at the Centre for Marine Magnetism of Southern University of Science and Technology. To separate the ferromagnetic contribution from raw hysteresis data, the high-field paramagnetic susceptibility was calculated and corrected using the 8,600 Series Magnetometer V1.3 program (Lakeshore Cryotronics, Inc.) by line fitting on the loop branch above 500 mT. Afterward, the ferromagnetic signal was smoothed at intervals of 10 mT. To further detect and evaluate the magnetic domain(s) for possible ferromagnetic materials in our samples, the first-order reversal curve (FORC) diagrams of six Muong Nong-type and four splash-form tektites were also measured using the same VSM 8604. FORC diagram were measured using a time interval of 0.5 s and a field increment of 2 mT, and the maximum applied field was 200 or 500 mT. The FORC data were processed using the FORCinel software with a VARIFORC smoothing algorithm (Harrison & Feinberg, 2008).

Natural remanent magnetization (NRM) of AASF tektites at South China was not reported before. Twenty-five Muong Nong-type and forty-nine splash-form tektites from South China were selected in this study to measure their NRM. The measurements were performed at the South China Sea Institute of Oceanology, Chinese Academy of Sciences, Guangzhou. A superconducting quantum interference device (SQUID) magnetometer (2G Enterprises, model 581DC, with sensitivity of 10^{-12} Am^2) that was installed in a magnetically shielded room (background field <500 nT) was employed. To qualitatively evaluate the order-of-magnitude of paleointensity recorded in our samples, the saturation isothermal remanent magnetization (SIRM) of eleven Muong Nong-type and thirty-four splash-form tektites were acquired after the measurements of NRM. The SIRM of these samples were acquired in a direct current (DC) field using a pulse magnetizer with 1 T. Afterward, the SIRM was measured using the same SQUID magnetometer. The ratio of equivalent magnetization (i.e., REM) is represented by NRM/SIRM ratio here, which follows earlier studies of paleointensity for igneous rocks and meteorites (e.g., Fuller et al., 1988; Gattacceca & Rochette, 2004). The purpose of REM is used to compare the order-of-magnitude of paleointensity for different types of tektites across AASF. To further investigate the unmixing magnetic coercivity distribution of our samples, we first measured the isothermal remanent magnetization (IRM) acquisition curves for three splash-form tektites using the VSM 8604 (maximum applied field of 1 T). Afterward, alternating field (AF) demagnetization was performed on these samples using the alternating demagnetizer (2G Enterprises, model 600). The stepwise increasing alternating field was up to 120 mT, and the increments were 2, 5 or 10 mT. After each step of AF demagnetization, the remanent magnetization of the sample was measured using the SQUID magnetometer. The unmixing magnetic coercivity distribution is calculated based on the MAX UnMix software (Maxbauer et al., 2016).

The IRM acquisition curves of the samples acquired using VSM 8604 exhibit erratic shapes (Section 3.2), possibly due to residual field-related instrumental noises and the low magnetization of the samples. Therefore, we additionally measured the IRM acquisition curves for three Muong Nong-type and three splash-form tektites from South China using a MC-1 pulse magnetizer and a 2G-RAPID cryogenic magnetometer (sensitivity of 1×10^{-12} Am^2). The magnetometer is installed in a magnetically shielded room that has a residual field of <300 nT. Samples were initially magnetized in a stepwise increasing DC field (up to 2 T), and their remanences after each step were measured. The orientation of each sample in the pulse magnetizer was fixed to be constant. Afterward acquiring the IRM at 2 T, each sample was rotated 180° along the DC field direction. We also obtained the back-field demagnetization curves using the MC-1 pulse magnetizer and the 2G-RAPID cryogenic magnetometer. The samples were initially magnetized in a stepwise increasing DC field (up to 1 T) and then their remanences after each step were measured. The above experiments were conducted at the Paleomagnetism and Geochronology Laboratory, Institute of Geology and Geophysics, Chinese Academy of Sciences in Beijing, China.

Anhysteretic remanent magnetization (ARM) of the tektites were analyzed, which is an effective method to detect the single-domain magnetic grains (King et al., 1983). It has been realized that the anisotropy of ARM of Muong Nong-type tektites at Laos and Thailand was minor (Gattacceca et al., 2021). For our experiment, the NRM of eight Muong Nong-type tektites were initially demagnetized in a stepwise increasing alternating field (up to 120 mT) using the 2G-RAPID cryogenic magnetometer. Then, the partial ARM was imparted in a stepwise increasing alternating field (up to 120 mT), and a 50 μT direct current biased field was superimposed using the 2G-RAPID cryogenic magnetometer. Finally, the total ARM was demagnetized in a stepwise increasing alternating field (up to 120 mT), and the AF increments were 2, 5 or 10 mT. The three procedures (i.e., NRM lost, ARM gained and ARM lost) had the same demagnetization steps and along the same *z*-axis of the sample. The orientation of each sample in the magnetometer was fixed to be constant. To further decode the potential magnetic domain(s) and coercivity

10.1029/2022JB025269

components of the tektite samples, we measured the AF demagnetization of NRM and SIRM for eight splash-form tektites using the 2G-RAPID cryogenic magnetometer. The NRM of the samples were initially demagnetized in a stepwise increasing alternating field (up to 40–90 mT). Afterward, a SIRM were acquired in a DC field using a pulse magnetizer with 2 T termed as $SIRM_{2T}$ here. The $SIRM_{2T}$ was then demagnetized in a stepwise increasing alternating field (up to 40–90 mT). The AF increments of 2 or 4 mT were used and the two procedures (NRM lost and SIRM lost) had the same demagnetization steps. The above measurements were also performed at the Paleomagnetism and Geochronology Laboratory, Institute of Geology and Geophysics, Chinese Academy of Sciences in Beijing, China.

We also selected three Muong Nong-type and three splash-form samples to study their low temperature magnetic behavior. The room temperature saturation isothermal remanent magnetization (RT-SIRM) and the low temperature saturation isothermal remanent magnetization (LT-SIRM), including the zero-field warming curves (ZFC) and the field warming curves (FC), were measured using a SQUID magnetometer (Quantum Design MPMS-3) at the Environmental Magnetism Laboratory of China University of Geosciences (Wuhan). The residual field of the superconducting solenoid after a magnet reset from 2.5 T during measurement is about 45 μT. The behavior of LT-SIRM acquired in a 2.5 T field at 10 K after cooling the sample from 300 to 10 K in zero field (ZFC) and in a 2.5 T field (FC) was monitored upon warming from 10 to 300 K in 5 K steps (Lagroix & Guyodo, 2017). The behavior of RT-SIRM acquired in a 2.5 T field was monitored while cycling from 300 to 10 K and back to 300 K in 5 K steps (Church et al., 2011).

2.4. Petrographic Observation

Among the analyzed samples, several Muong Nong-type tektites exhibited magnetic signals that indicate the possible existence of pseudo-single domain (PSD) magnetic grains, and such signals did not occur in any of our analyzed splash-form tektites (Section 3.2). These Muong Nong-type tektites may contain comparatively large ferromagnetic minerals, and we prepared random thin sections from these samples for petrographic observations. The sections were about 1 mm thick and 5 by 7 mm long. After polishing the sections, we were able to identify several opaque inclusions in the glass under reflected and transmitted light of stereoscopes.

One of these Muong Nong-type tektites contain abundant whitish opaque materials in the glass (Section 3.3). Featuring diffuse margins, the opaque materials were un-melted components in the tektite melt. To evaluate the shock level of these materials, a Thermo micro-Raman spectrometer was used at the Purple Mountain Observatory, Chinese Academy of Sciences. Raman spectra were acquired using a 532 nm unpolarized laser with power of 6 mW. The total analytical time was 60 s. The Raman spectra for these whitish opaque materials showed that they are dominated by α-quartz, suggesting a relatively low shock level of precursor materials that formed this sample (Section 3.3). Afterward, we obtained a high-resolution three-dimensional (3D) tomography for this sample to locate relatively large (still micro-sized) and dense particles that appeared brighter than the surrounding glass matrix. These particles are likely metallic materials that might contribute to the magnetic properties of this sample. The Carl Zeiss Xradia 520 Versa High Resolution X-ray Tomographic Microscope (HR-XRTM) at the micro-CT lab of the Nanjing Institute of Geology and Palaeontology, Chinese Academy of Sciences was employed. The scanner was set up to 70 kV voltage 6 W power. A total of 1,015 projections were collected over a rotation of 360° and producing a voxel dimension of ∼0.35 μm for the sample. Inspecting the backscattered electron images that were sliced from the 3D tomography, we extracted the accurate coordinates for the relatively large dense particles. We then prepared thin sections for these particles according to their coordinates. Stereoscopes were used to examine the sections to locate the iron-bearing particles, and the particles were then gradually exposed by polishing for compositional analyses. The carbon coated thin sections were then delivered into the LYRA 3 XMU Field Emission Scanning Electron Microscope (SEM) at the Guangdong University of Technology for surface morphology observation. These thin sections were delivered into the JEOL JXA-iSP 100 Electron Probe Micro Analyzer (EPMA) at the Southern Marine Science and Engineering Guangdong Laboratory (Zhuhai) for composition analyses. The operation conditions involved a 15 kV acceleration voltage, a 20 nA probe current, and a beam diameter set to 1 μm for target particles. The detection limits were ∼0.01 wt% for all the elements.

3. Results

3.1. XRF Composition

We confirm that our sampled glasses belong to AASF based on both their stratigraphic occurrences (Section 2.1) and their compositional comparison with the five major Cenozoic strewn fields of tektites on Earth. The major elements of the eight samples (Table 1) are consistent with those of AASF tektites, and they are distinctively different from those of the other Cenozoic strewn fields (Figure 3).

3.2. Rock Magnetic Properties

Both Muong Nong-type and splash-form tektites from South China exhibit strong paramagnetic signals as evident by the linear uncorrected hysteresis loops (insets of Figure 4). Earlier geochemical (Schreiber et al., 1984) and magnetic studies (e.g., Rochette et al., 2015) revealed that the dominating paramagnetic signal of AASF tektites is mainly caused by dispersed Fe^{2+} ions, which were ascribed to fast cooling of the impact melt in a reducing environment (Costa et al., 2014; Koeberl, 1992).

After subtracting the paramagnetic contribution, the corrected hysteresis loops of all the samples exhibit weak ferromagnetic signals. Figure 4 shows the results, and Figure S2 in Supporting Information S1 shows similar results for additional six splash-form tektites. Due to the rather weak saturation remanence (10^{-7}–10^{-6} Am^2/kg) of the samples (Table 2), the corrected hysteresis loops exhibit obvious noises at high fields, reflecting difficulties of completely excluding contributions by the dominating paramagnetic component (Paterson et al., 2018; Rochette et al., 2015, 2019). It is notable that some of the corrected hysteresis loops are apparently not closed at high fields (e.g., Figures 4c and 4f and Figure S2d in Supporting Information S1), and similar phenomena was observed for Muong Nong-types tektites from Indochina, which was ascribed to the strong paramagnetic signal of the samples (Rochette et al., 2019).

While the splash-form tektites from South China do not exhibit wasp-waisted hysteresis loops (Figures 4d–4f), the Muong Nong-type tektites show wasp-waisted hysteresis loops (Figures 4a–4c) that are consistent with those formed by PSD magnetite and/or a mixture of PSD and multidomain (MD) magnetite (Roberts et al., 1995). Similar wasp-waisted hysteresis loops were also observed for Muong Nong-type tektites from southern Laos, which were interpreted to be caused by PSD magnetite (Gattacceca et al., 2021).

The IRM acquisition curves of most splash-form tektites and Muong Nong-type tektites from South China show stable increase before 150–200 mT and reach 95% of SIRM before 300 mT (Figure 5), indicating that low-coercivity magnetic mineral(s) dominates the IRM variations. The IRM acquisition curves of the three splash-form tektites exhibit relatively erratic shapes at higher fields (Figures 5d–5f). For low magnetization samples, such erratic IRM acquisition curves obtained at room temperature were noticed in Greenland glacier ice, which were ascribed to minor amounts of superparamagnetic (SP) grains in the samples (Lanci et al., 2001; Lanci & Kent, 2006). Due to the possible effect of thermal relaxation, such IRM acquisition curves are not suitable for performing unmixing coercivity analyses (Heslop et al., 2004). For comparison, the IRM acquisition curves of the three Muong Nong-type tektites exhibit relatively stable shapes, indicating a weaker thermal relaxation in the Muong Nong-type tektite samples than that in the splash-form tektites. In the backfield demagnetization curves of SIRM (Figure 5), the coercivity of remanence (B_{cr}) of the Muong Nong-type tektites and splash-form tektites is about 31–86 mT, suggesting the presence of low-coercivity magnetic mineral(s). However, the B_{cr} of the splash-form tektites, acquired by both VSM 3900 and VSM 8604, cannot be extracted due to their much lower magnetization (Table 2 and Figure S3 in Supporting Information S1). See Text S1 in Supporting Information S1. The low magnetization of our samples also yielded overwhelmingly large noises in their FORC diagrams (Figures S5–S6 in Supporting Information S1), preventing reliable extraction of possible ferromagnetic signals (see Text S3 in Supporting Information S1).

On the Day plot (Figure 6), the hysteresis ratios of all the analyzed Muong Nong-type samples (Table S4 and S5 in Supporting Information S1) are constrained in the PSD area, consistent with their wasp-waisted hysteresis loops (Figures 4a–4c). Earlier investigations for Muong Nong-type tektites at Laos and Thailand yielded similar results, with an additional sample that contain MD grains (Figure 6; Gattacceca et al., 2021). It is notable that a mixture of MD magnetite and SD magnetite can also cause hysteresis ratios that are constrained in the PSD area (Dunlop, 2002). In addition, Werner and Borradaile (1998) measured the hysteresis ratios for five indochinites with unknown types, indicating the existence of PSD grains (Figure 6). Considering that the remanence of splash-form tektites from both South China (this study) and Australia (Werner & Borradaile, 1998) is much weaker, the five indochinites measured by Werner and Borradaile (1998) most likely belong to the Muong Nong-type.

To further decode the magnetic carrier(s) in the Muong Nong-type tektites from South China, we investigated their acquisition curves of partial anhysteretic remanent magnetization (pARM) and the AF demagnetization

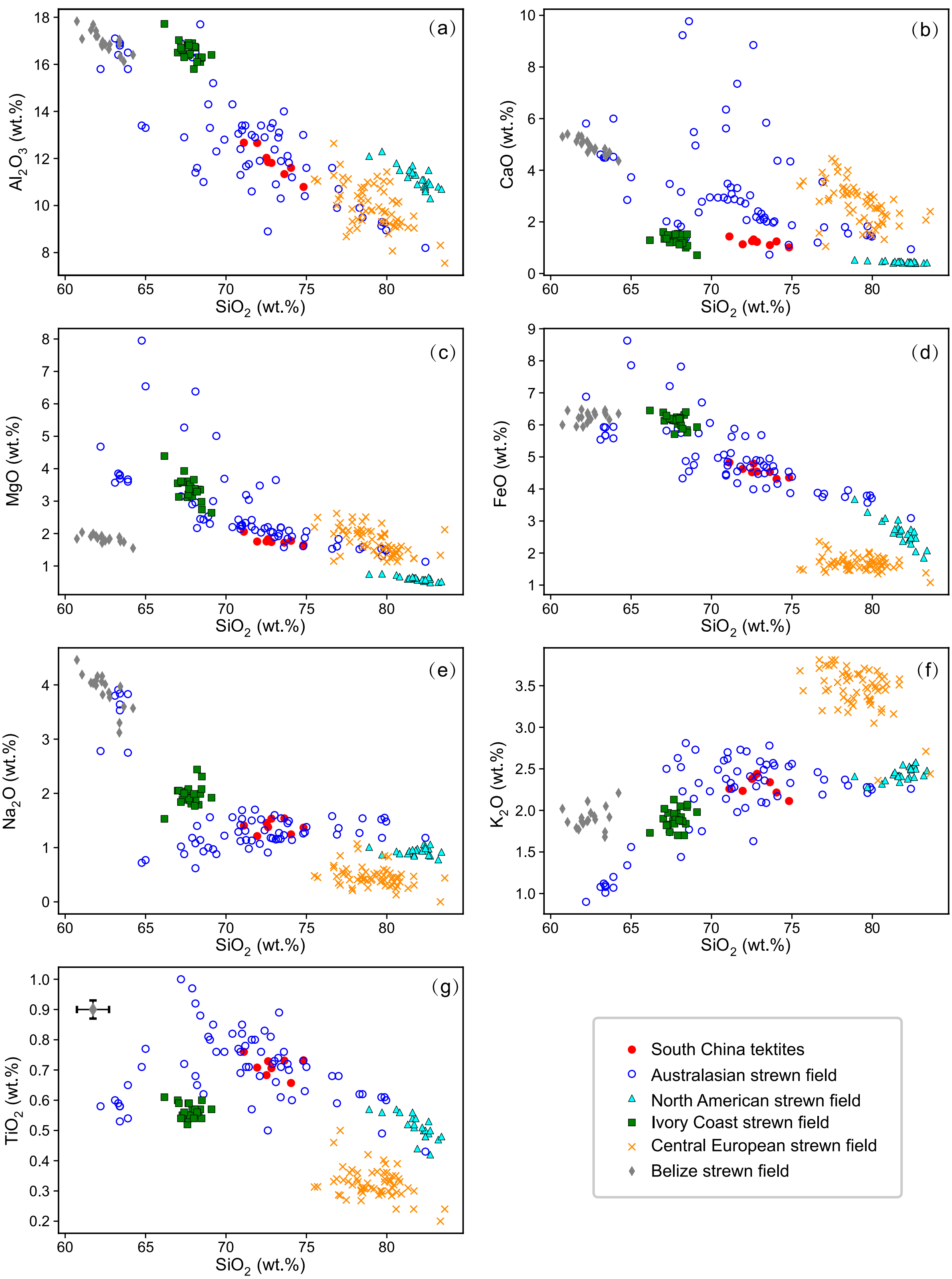

Figure 3. Harker diagrams comparing the contents of major elements for tektite samples from South China and those from the five major types of Cenozoic strewn fields. Published data from Philpotts and Pinson (1966), Chapman and Scheiber (1969), Cuttitta et al. (1972), Koeberl et al. (1997), Albin et al. (2000), von Engelhardt et al. (2005), Ackerman et al. (2020), and Koeberl et al. (2022).

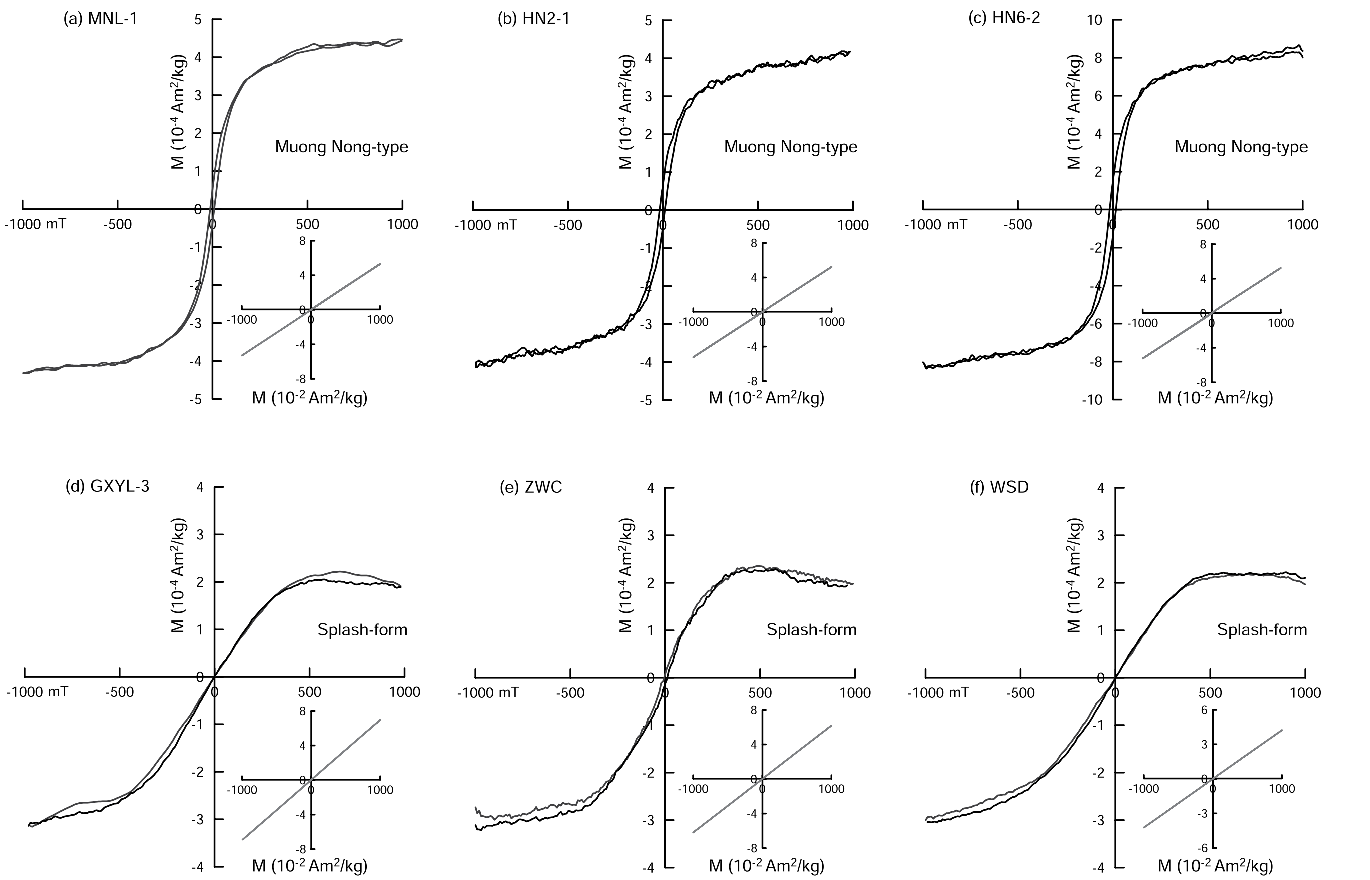

Figure 4. Hysteresis loops for AASF tektites from South China. (a–c) Muong Nong-type tektites. (d–f) Splash-form tektites. Inserted graphs are primary hysteresis loops before paramagnetic correction, in which *M* is the abbreviation for magnetization.

Table 2
Magnetic Parameters of Australasian Tektites

Subareas	Type	χ (10^{-9} m^3/kg)	χ_{fd}%	M_s (10^{-4} Am^2/kg)	M_{rs} (10^{-6} Am^2/kg)	B_c (mT)	B_{cr} (mT)	NRM (10^{-6} Am^2/kg)	NRM/SIRM (%)
South China	MN	46.6 (21.4–66.1)	0.03 (0.005–0.28)	4.29 (0.37–9.16)	32.3 (6.1–136)	9.45 (3.97–16.2)	26.7 (1.12–61.4)	2.4 (0.08–14.1)	6.4 (0.8–22)
South China	SF	74 (35.4–106.1)	0.05 (0.005–0.68)	2.71 (0.06–7.86)	8.25 (1.56–19.2)	7.2 (2.33–19.6)	–	0.016 (0.001–0.1)	0.8 (0.2–2.8)
Thailand, Laos[a]	MN	93 (77.3–147.3)	0.52 (0.24–0.7)	41 (8–131)	55.2 (7.9–120)	15.2 (0.8–19.4)	35 (27–45)	2.8 (0.03–19.7)	5 (0.5–58)
Philippinites[b]	SF	94 (78.2–129)	–	–	4.9 (0.7–9)	–	–	0.18 (0.1–0.27)	1.2 (1.0–1.4)
Australia[b]	ASF	86 (71.3–103.5)	–	–	–	–	–	0.04 (0.05–0.1)	0.9 (0.7–1.1)
Indonesia[a]	SF	102 (81.3–125.4)	–	–	–	–	–	–	–

Note. The average values and value ranges (in squares) are shown here, and the raw data for each of the measurement were provided in Tables S2, S3 and Tables S4, S5 in Supporting Information S1. χ = Low-field magnetic susceptibility; χ_{fd}% = frequency-dependent susceptibility; M_s = saturation magnetization; M_{rs} = saturation remanence; B_c = coercivity; B_{cr} = coercivity of remanence. MN = Muong Nong-type; SF = splash-form; ASF = ablated splash-form.

[a]Data from de Gasparis et al. (1975), Rochette et al. (2019), and Gattacceca et al. (2021). Note that two abnormally large M_{rs} and M_s were reported by Gattacceca et al. (2021), and the two values are excluded during the calculation of the average values. [b]Data from Rochette et al. (2019) and Donofrio (1977).

10.1029/2022JB025269

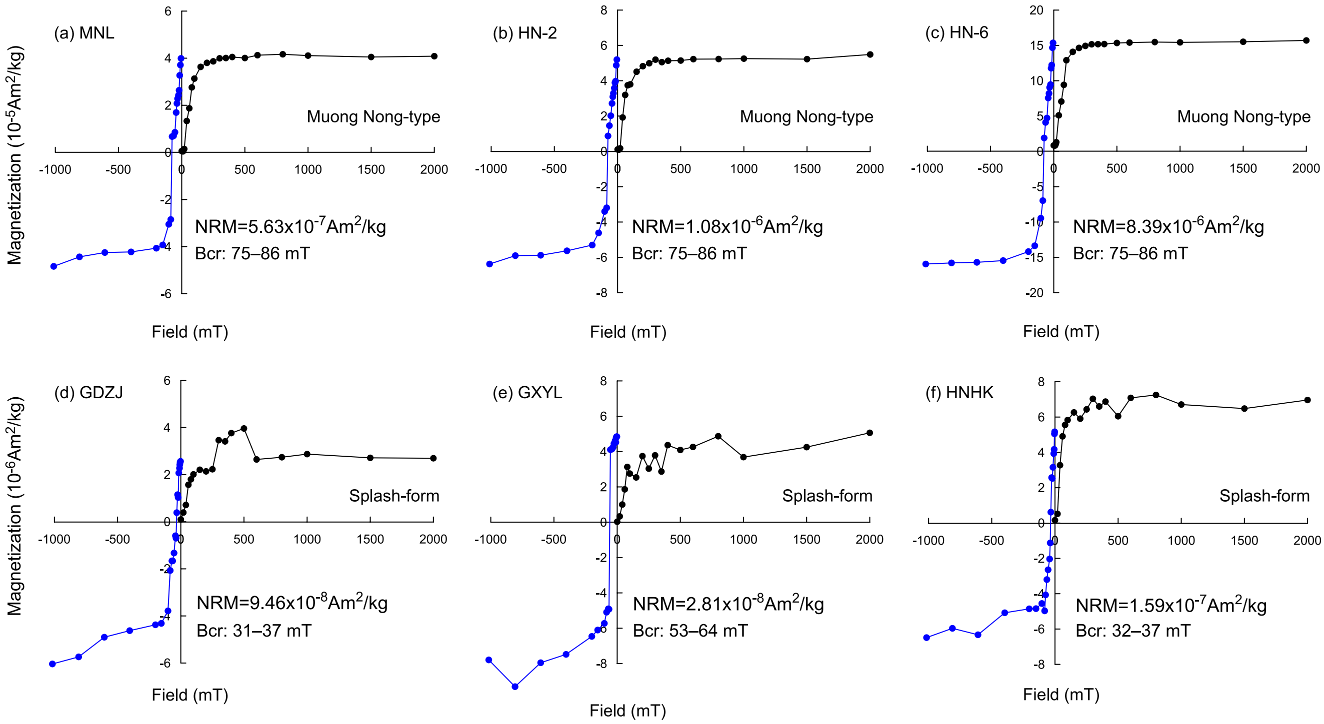

Figure 5. IRM acquisition curves (black) and backfield demagnetization of SIRM curves (blue) for three Muong Nong-type tektites samples and three splash-form tektites from South China. (a–c) Muong Nong-type tektites. (d–f) Splash-form tektites. All the IRM acquisition curves and backfield demagnetization of SIRM curves shown here are measured using a pulse magnetizer and a 2G-RAPID cryogenic magnetometer.

of ARM curves. Most of the samples yield regular pARM acquisition curves and AF demagnetization curves of ARM, and the median destructive field (MDF) can be determined (22–40 mT). The average MDF of the total ARM is 27 mT (Figure 7), which it is comparable with that of SD and/or PSD magnetite (~15–31 mT, Johnson et al., 1975; Yu et al., 2002). Considering that the Day plot reveals no signals of SD particles in the Muong Nong-type tektites (Figure 7) and magnetic properties of PSD magnesite can be similar with those of SD magnetite (Roberts et al., 2018), the two lines of evidence indicate that the PSD grains in the Muong Nong-type tektites are likely PSD magnetite, which is consistent with the interpretation of Gattacceca et al. (2021).

The Muong Nong-type tektites from South China exhibit a distinct Verwey transition signal around 120 K in the FC and ZFC curves (Figures 8a–8c), indicating the presence of magnetite (e.g., Kosterov, 2001). This observation is supported by the decay of RT-SIRM curves at about 120 K during cooling (Figures 8d–8f), which is consistent with signals formed by magnetite (e.g., Smirnov & Tarduno, 2011). However, measurements of temperature dependence of magnetic susceptibility for the Muong Nong-type tektites yield no distinct Hopkinson peaks of magnetite or other ferromagnetic minerals (Figure S7 in Supporting Information S1), suggesting a relatively low content of magnetite in these samples. The RT-SIRM curves show distinct upturns from 90 to 10 K (Figures 8d–8f), and this feature is inconsistent with that formed by magnetite (Lagroix & Guyodo, 2017; Smirnov & Tarduno, 2011). The steep upturn is ascribable to the low-temperature behavior of the dominating paramagnetic component in these tektites (Nayak et al., 2018), as antiferromagnetic interactions of the Fe ions would enhance significantly at 5–50 K, causing sharp increase of remanent magnetization toward lower temperature in a small residual field (Aubourg & Pozzi, 2010; Coey & Ghose, 1988; Kars et al., 2011; Nayak et al., 2018). Alternatively, it has also been well-recognized that thermal unblocking of (super)paramagnetic particles at low temperatures (from about 10 to 90 K) would also cause sharp drops in magnetic moment (Geiss et al., 2004; Moskowitz et al., 1989; Starunov et al., 2019).

The splash-form tektites from South China exhibit different low-temperature magnetic behavior than the Muong Nong-type tektites (Figure 9). Both the LT-SIRM (Figures 9a–9c) and RT-SIRM (Figures 9d–9f) of the splash-form tektites show exponential decay of remanent magnetization with increasing temperature, and no obvious Verwey transition of magnetite is visible around 120 K (Figures 9a–9c). The sharply enhanced magnetization toward

10.1029/2022JB025269

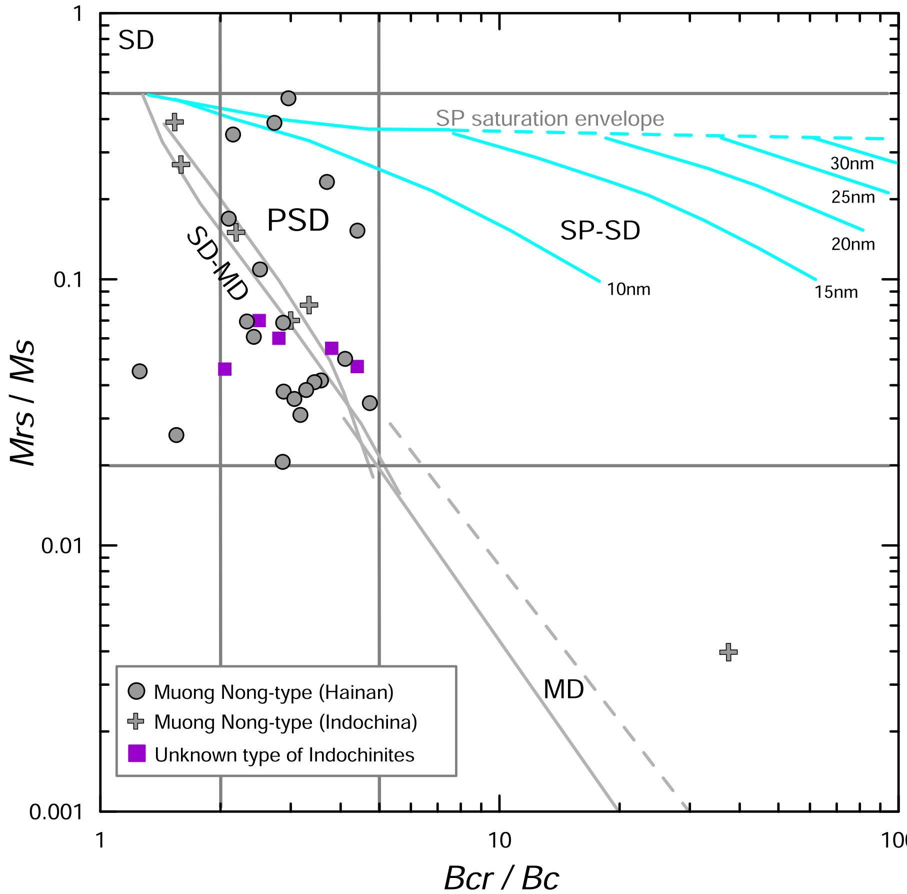

Figure 6. Day plot (Day et al., 1977; Dunlop, 2002) comparing the hysteresis ratios of Muong Nong-type tektites from South China (gray circles) and elsewhere of AASF. Data for the earlier-measured six Muong Nong-type indochinites (gray crosses) are referred from Gattacceca et al. (2021), and those for the five indochinites (purple squares) were referred from Werner and Borradaile (1998).

low temperature (<90 K; Figure 9) is consistent with the strong effect of the dominating paramagnetic signal. The remanent magnetization of our splash-form tektites decreases by about 94% from 10 to 300 K (Figure 9), and the finite values of remanence at 300 K indicate the existence of minor amounts of stable remanence carriers (Moskowitz et al., 1989). For comparison, Senftle et al. (1964) performed low-temperature magnetic susceptibility analyses for splash-form tektites from the Philippines, and positive intercepts at the susceptibility axis were noticed, which were interpreted to be caused by a residual temperature-independent constituent. Such signal of ferromagnetic materials was believed to be formed by finely-dispersed (e.g., 1–100 nm) metallic spherules in the glass matrix (Senftle et al., 1964).

We selected eight splash-form tektites to obtain their stepwise demagnetization of NRM and $SIRM_{2T}$ in a stepwise increasing alternating field (up to 90 mT). Their NRM curves exhibited erratic shapes due to their low magnetization (blue curves in Figure 10). Most of the NRM curves decreased by 80%–90% at an alternating field of less than about 20–30 mT, but the sample shown in Figure 10e retained 18% of its NRM above an alternating field of 90 mT. The $SIRM_{2T}$ of most samples have more regular shapes (red curves in Figure 10). They exhibit similar demagnetization behaviors with their counterpart NRM demagnetization curves, but the sample shown in Figure 10b retained 16% of its primary SIRM above an alternating field of 40 mT. Therefore, soft magnetic component(s) that have different coercivities commonly exist in the splash-form tektites. The MDF of SIRM is about 3–16 mT, and most of them are larger than 9 mT (Figure 10). For comparison, the MDF of SIRM for SD magnetite is about 5–17 mT (Johnson et al., 1975; Maher, 1988). Therefore, the soft magnetic components in the splash-form tektites may contain SD magnetite. Considering that the splash-form samples exhibit no distinct Verwey transition signal around 120 K in the FC or ZFC curves (Figures 9a–9c) and no obvious Hopkinson

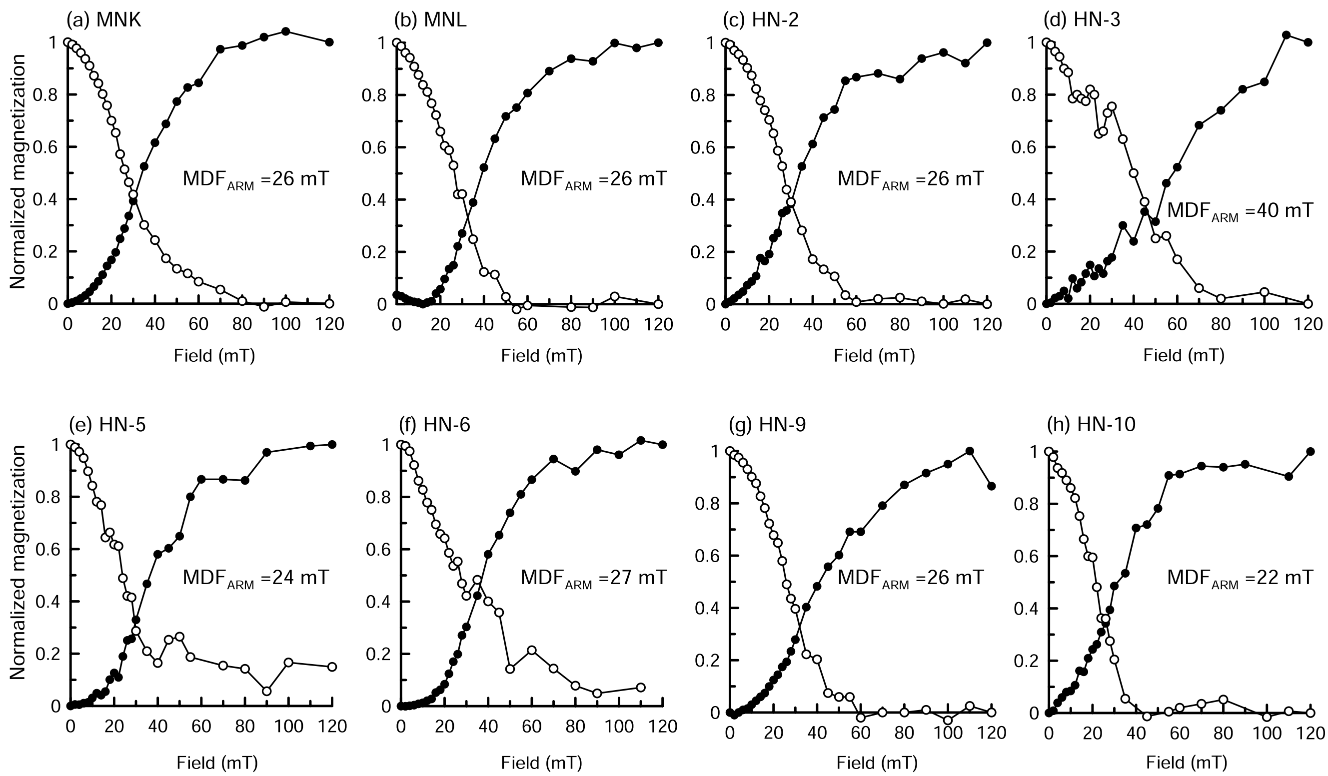

Figure 7. Partial ARM acquisition curves (black circles) and AF demagnetization of ARM curves (hollow circles) of the Muong Nong-type tektites from South China. MDF = median destructive field.

peak of magnetite was observed neither (Figure S7 in Supporting Information S1), SD magnetite may be rather minor in the samples. Meanwhile, as indicated by their AF demagnetization curves (Figure 10), signals formed by components that have lower coercivities than SD magnetite may also exist in the splash-form tektites. This implication is also consistent with both the stable increase of IRM acquisition curves at relatively low fields (Figures 5d–5f) and the preliminary analyses based on unmixing magnetic coercivity for the AF demagnetization of SIRM (Figure S4 and Text S2 in Supporting Information S1). Note that the AF demagnetization curves of SIRM for splash-form tektites are also rather irregular due to the low magnetization of the samples, but they are relatively reliable compared to their IRM acquisition curves obtained at room temperature (Figure 5 and Figure S3 in Supporting Information S1).

3.3. Locating and Resolving Magnetic Particles in AASF Tektites

Although metallic particles that are as large as 100 μm were reported in a few splash-form tektites from the Philippines (Chao et al., 1962, 1964; Donofrio, 1977), it is generally believed that microscopic metallic particles that are visible in optical microscopes are extremely rare in AASF splash-form tektites (Rochette et al., 2015; Thorpe & Senftle, 1964). We find that the AASF splash-form tektites from South China are dominated by paramagnetic signals that may contain additional weak signals of trace amounts of SD magnetite (Figure 10), indicating that the chance of finding microscopic metallic particles via optical microscopes is small. Therefore, our petrographic investigation of magnetic particles in AASF tektites from South China was mainly focused on the Muong Nong-type tektites shown in Figures 2e–2g, which exhibit relatively obvious signal of PSD magnetite.

Five random thin sections were sawed from the two tektites shown in Figures 2f and 2g, and the polished sections were examined under stereoscopes to locate heterogenous materials and for further identifying possible magnetic materials using EPMA. The Muong Nong-type tektite shown in Figure 2e show many whitish opaque materials on the exposed section, which appear as un-melted mineral/lithic fragments considering their diffuse boundaries (Figures 11a and 11b). Our Raman spectroscopy investigation shows that the whitish opaque materials are dominated by α-quartz (Figure 11c). Similar occurrence of un-melted quartz was also reported in a Muong Nong-type

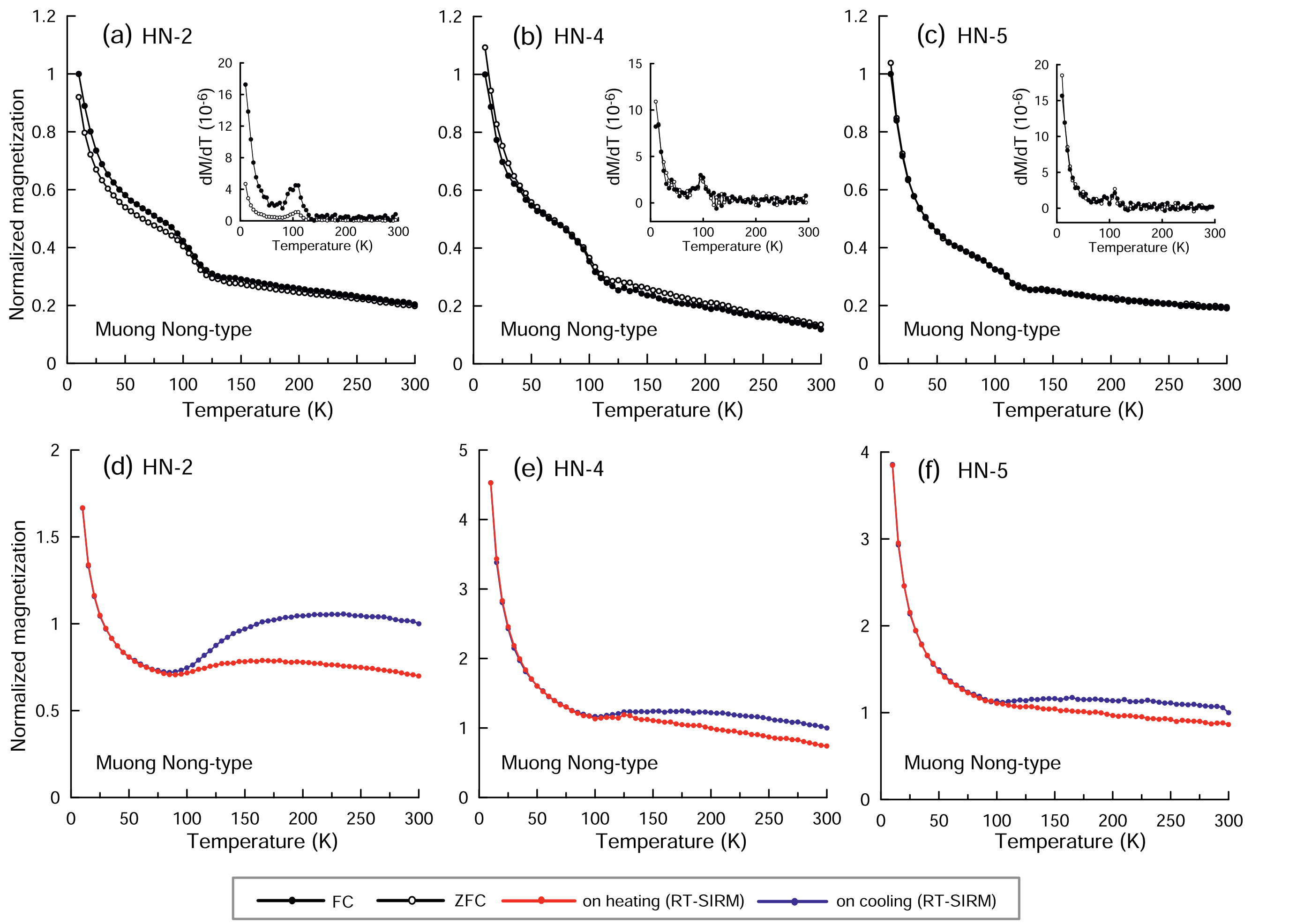

Figure 8. Low-temperature magnetic behavior of AASF Muong Nong-type tektites from South China. (a–c) The ZFC and FC of Muong Nong-type samples. Inserted graphs are the first derivative curves. The remanence values are normalized to the initial ZFC and FC value at 10 K. (d–f) The RT-SIRM of Muong Nong-type tektites are cooled to 10 K (blue circles) and warmed back to 300 K (red circles). The remanence values are normalized to the initial RT-SIRM. Low-temperature magnetic data could be found in Table S6.

tektite from Laos (Glass et al., 2020), indicating that its shock level was relatively low compared to the other Muong Nong-type tektites. Therefore, the sample shown in Figure 11a has a large probability of preserving former magnetic materials in the pre-impact target. We obtained the three-dimensional structural information for this sample using HR-XRTM, locating at least six micron-sized relatively dense inclusions (Figure 11d). Thin sections prepared by sawing successfully exposed several relatively large inclusions (Figures 11e, 12a, and 12c), and their compositions were then investigated using EPMA.

The particles have diameters of about 9.8–13.5 μm, and they occur as black and opaque particles under both reflected and transmitted light of stereoscopes (Figure 12). Featuring distinctive boundaries with the host glass, the particles exhibit circular shapes in the exposed sections (Figure 13). Our EPMA measurements reveal that the relative dense particles are mainly composed of Fe and S, and minor amounts of Ti, Ni, Co, Cr, and Mg are detected (Table 3). Metallic spherules with similar morphology and compositions were also observed in impact glasses formed by the Bosumtwi and Ries craters (El Goresy, 1966; Stähle, 1972). The morphology and compositions of the Fe-S spherules are consistent with being formed due to immiscibility of silicate and metallic melt during cooling (Belkin & Horton, 2009; Hamann et al., 2017; Reid et al., 1964). It is notable that the accuracy of the EPMA results is not as good as measurements for regular rock samples (uncertainty up to 5 wt%; Table S7 in Supporting Information S1). This issue was noticed before in EPMA measurements for metallic spherules in Muong Nong-type tektites from Laos (Krizova et al., 2019), which was ascribed to the small sizes of the particles.

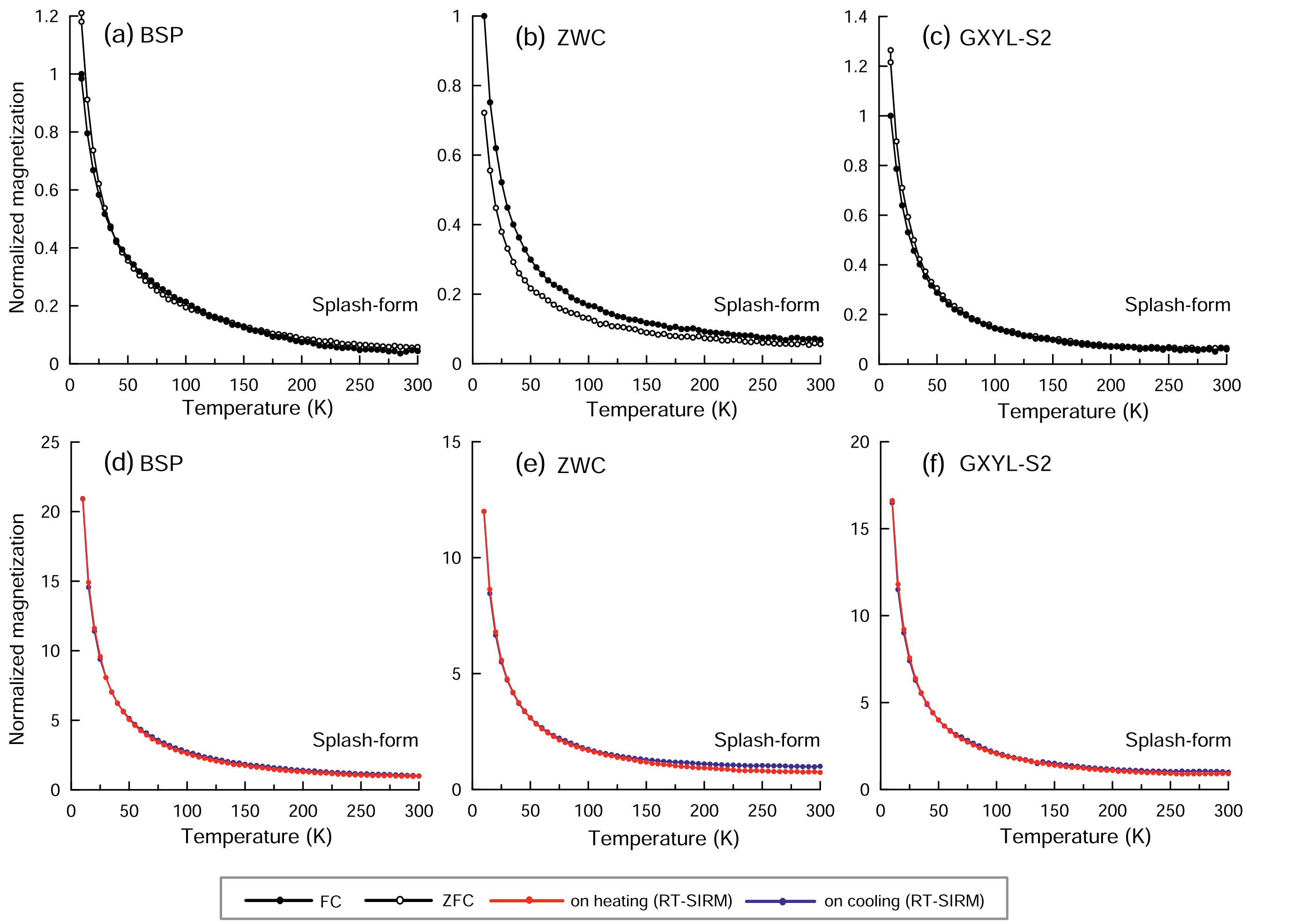

Figure 9. Low-temperature magnetic behavior of AASF splash-form tektites from South China. (a–c) The ZFC and FC of splash-form tektites. The remanence values are normalized to the initial ZFC and FC value at 10 K. (d–f) The RT-SIRM of splash-form tektites are cooled to 10 K (blue circles) and warmed back to 300 K (red circles). The remanence values are normalized to the initial RT-SIRM. Low-temperature magnetic data could be found in Table S6.

4. Discussion

4.1. Comparison of Magnetic Properties for AASF Tektites at Different Areas

4.1.1. Comparison of Magnetic Susceptibility

Comparison of magnetic susceptibility of AASF tektites from South China and the other areas reveals much larger variations than earlier observations. Figure 14 and Table 2 show the summary of the comparison. On average, tektites from South China exhibit lower magnetic susceptibility than those from the other areas. Especially, the average magnetic susceptibility of the Muong Nong-type tektites from South China (46.6×10^{-9} m^3/kg) is the lowest in the entire strewn field, and it is obviously less than that of Muong Nong-type tektites from Laos and Thailand (Figure 14a), while the latter is slightly larger with that of the splash-form tektites from South China (74×10^{-9} m^3/kg). Tektites from Australia, Vietnam, the Philippines (blue dots in Figure 14a) and Indonesia (orange dots in Figure 14a) exhibit the largest average magnetic susceptibility (Table 2). It is also notable that for the same morphological type of tektites from a given geographic area, their magnetic susceptibility exhibits variations up to several folds, such as the splash-form tektites from South China (Figure 14a).

Paramagnetic component is the major and/or dominating contribution to the magnetic susceptibility of different types of AASF tektites at various locations (Gattacceca et al., 2021; Rochette et al., 2015, 2019). Dispersed Fe^{2+} ions in tektites are believed to be the major cause of the paramagnetic signal of AASF tektites (Rochette et al., 2015). The above comparison may indicate that the average concentration of Fe^{2+} ions is different in AASF

10.1029/2022JB025269

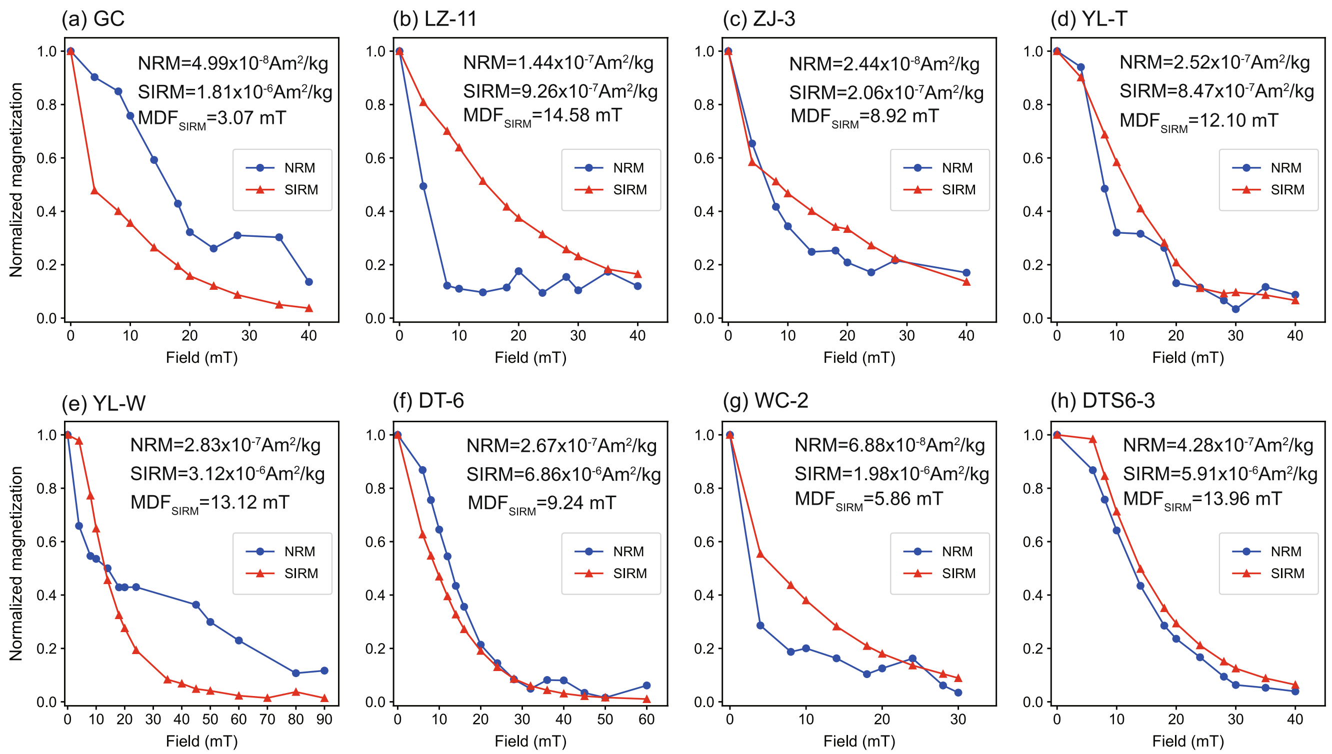

Figure 10. AF demagnetization curves of NRM (blue) and $SIRM_{2T}$ (red) for AASF splash-form tektites from South China. MDF = median destructive field.

tektites with different morphological types and from various locations. A possibly lower concentration of Fe^{2+} ions in Muong Nong-type tektites than splash-form tektites is supported by earlier geochemical studies. While Fe in AASF tektites is dominated by Fe^{2+} (Koeberl, 1992), Muong Nong-type tektites contain a lower ratio of Fe^{2+}/Fe^{3+} than both splash-form and ablated splash-form tektites (Costa et al., 2014; Giuli et al., 2002). This geochemical characteristic was interpreted to be caused by a less reduced environment during the formation of the Muong Nong-type tektites (Costa et al., 2014).

4.1.2. Comparison of Saturation Remanence and Coercivity

Our Muong Nong-type tektites generally exhibit larger saturation remanence (M_{rs}) than the splash-form tektites from South China (Figure 14b), with a difference of about 4 times (Table 2). The M_{rs} of Muong Nong-type tektites from Laos and Thailand are generally comparable with those from South China (Figure 14b, Table 2), with two samples from Laos and Thailand exhibit exceptionally large M_{rs} (gray crosses the up-right corner of Figure 14b). Only a handful of ablated splash-form tektites from Australia have reported M_{rs} (Donofrio, 1977), and their values are within the range of M_{rs} for the splash-form tektites from South China (Table 2). Therefore, the content of ferromagnetic materials in australites and splash-form tektites from South China is among the lowest in the entire strewn field, while that in the Muong Nong type tektites is generally larger and it does not exhibit obvious regional variations.

The coercivity values (B_c) for AASF splash-form and Muong Nong-type tektites are mostly comparable (Table 2) and they are less than 20 mT, suggesting that the coercivity is mainly caused by soft magnetic components. This result is consistent with the other measurements that showed the existence of minor amounts of PSD magnetite in our Muong Nong-type tektites (Figure 7) and trace amounts of SD magnetite in our splash-form tektites (Figure 10).

4.1.3. Comparison of Natural Remanent Magnetization and Ratio of Equivalent Magnetization

We present the first report of NRM (Figure 14c) and NRM/SIRM ratio (i.e., REM; Figure 14d) for AASF tektites from South China, and their comparisons with those from the rest of the strewn fields. In a given geographic area, each morphological type of tektites exhibits large variations in both their NRM and REM (Figures 14c–14d). In general, Muong Nong-type tektites from South China exhibit similar NRM with those from Thailand and southern Laos (de Gasparis et al., 1975; Gattacceca et al., 2021). Their average values are about 150 times larger than that of splash-form tektites at South China (Table 2), while the latter is comparable with that of australites

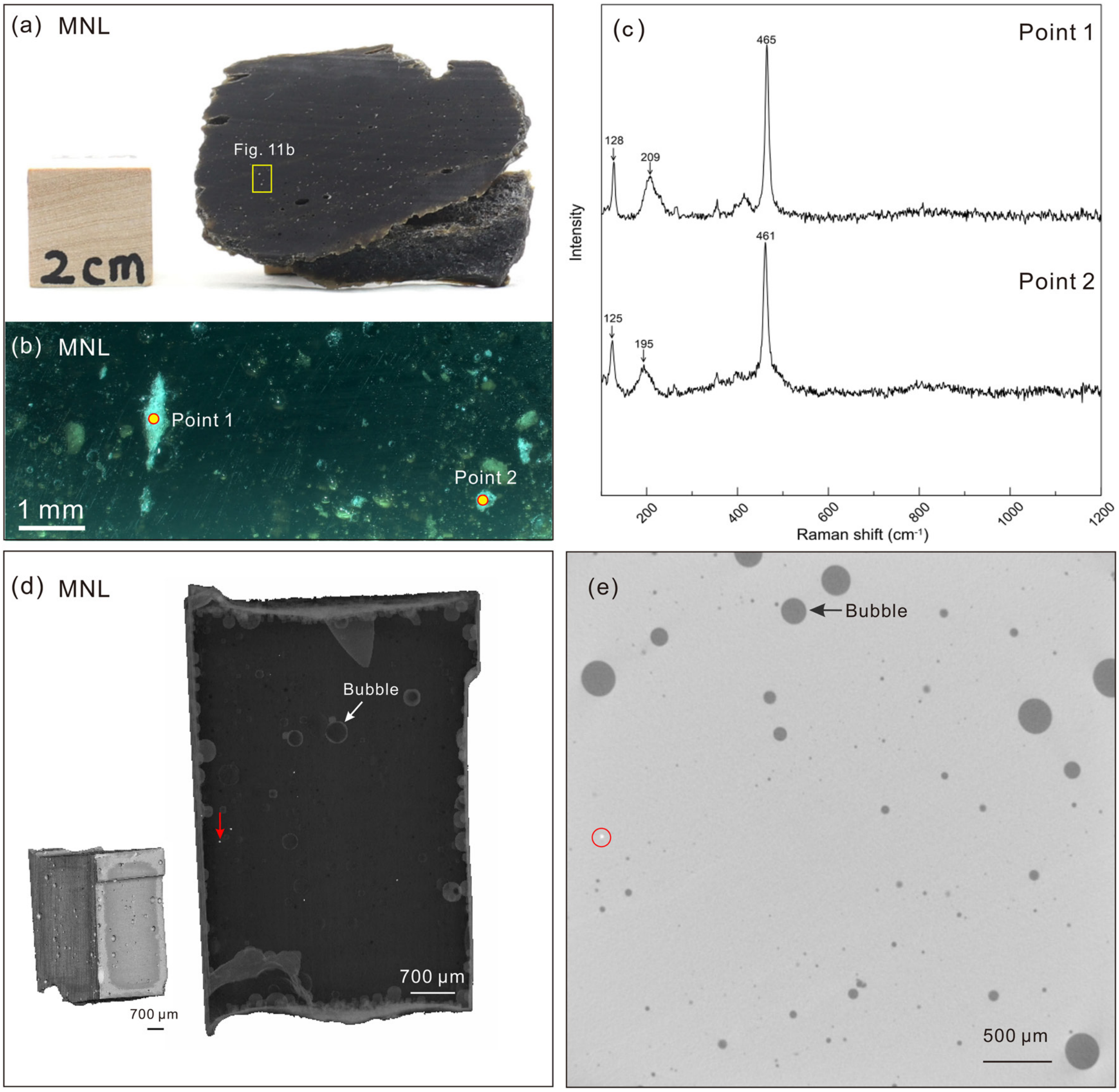

Figure 11. Relatively dense particles in a Muong Nong-type tektite as revealed by 3D tomography using HR-XRTM. (a) Exposed interior of a Muong Nong-type tektite from Hainan (MNL) showing abundant whitish opaque materials in the glass. (b, c) Raman spectroscopy observation showing that the white materials are dominated by α-quartz. (d) At least six particles that are denser than the surrounding glass matrix are visible in the high-resolution 3D reconstruction (inset) for this sample. (e) A slice from the 3D model for a relatively large dense particle (red arrow in panel d) that appear brighter than the surrounding glass.

but slightly less than that of philippinites (Figure 14c). Note that available measurements for philippinites and australites are sparse (Donofrio, 1977). The observed NRM values appear to be positively correlated with those of M_{rs} and SIRM (Figure 14c and Figure S8a in Supporting Information S1), indicating that the content of ferromagnetic materials is an important issue for the natural remanent magnetization of AASF tektites.

As an order-of-magnitude estimation for paleointensity, REM is not substantially affected by the content of ferromagnetic materials (Cisowski et al., 1975; Tauxe, 1993; Wasilewski & Dickinson, 2000), which is supported by the weak correlation between REM and SIRM or M_{rs} of the AASF tektites from South China (Figure S8b and S8c in Supporting Information S1). See Text S4 in Supporting Information S1. For comparison, the REM and NRM of AASF tektites exhibit positive correlation (Figure 14d), suggesting that REM is a reliable indicator of paleomagnetic field information recorded in the NRM. In general, REM of the Muong Nong-type tektites from South China is comparable with that Muong Nong-type tektites from Laos and Thailand, which is larger than that of australites and splash-form tektites from South China and elsewhere (Figure 14d). Table 2 shows the comparison of the range and average values of REM. On average, splash-form tektites from South China have the lowest REM in the entire strewn field (Figure 14d and Table 2).

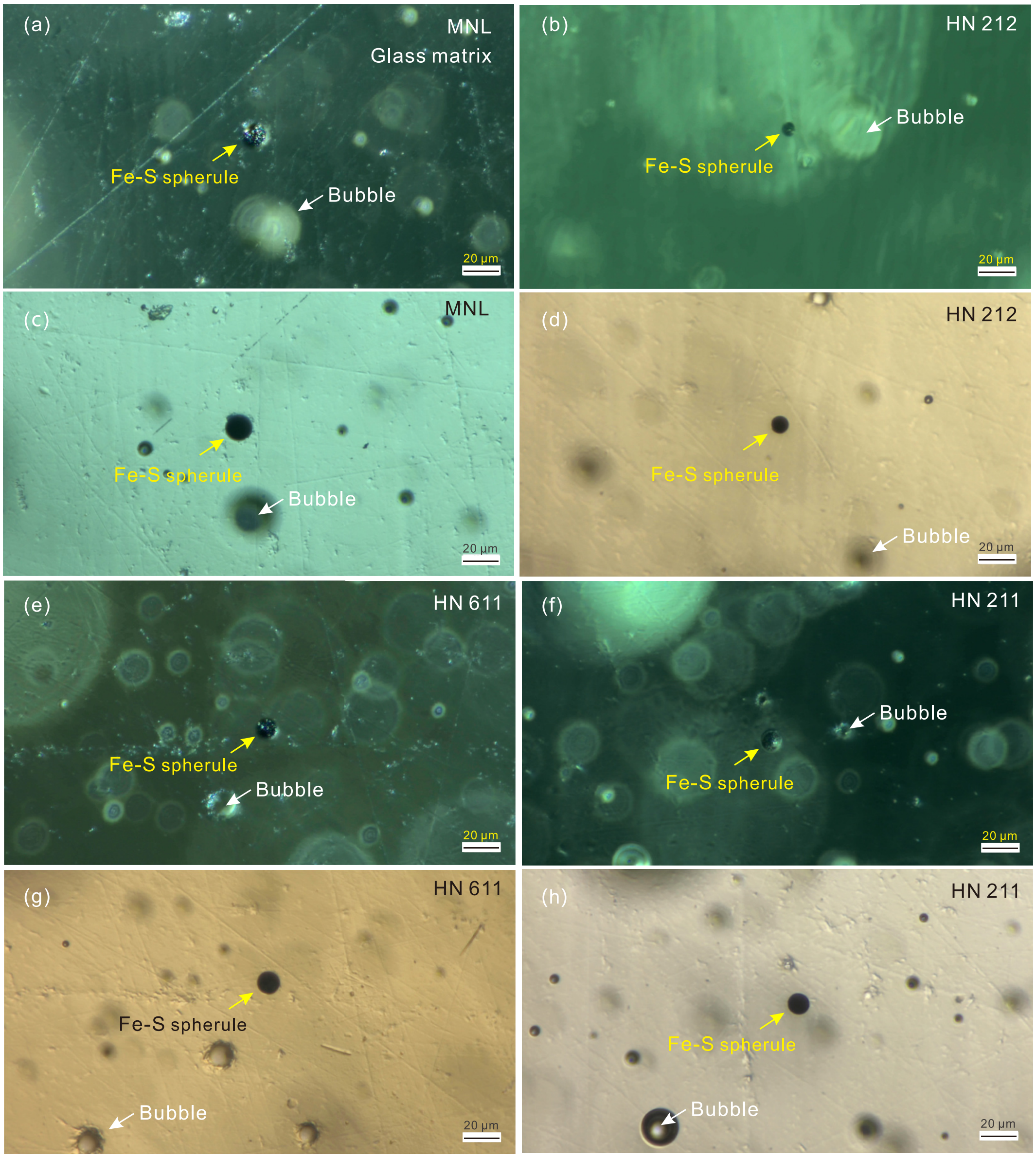

Figure 12. Optical images for Fe-S spherules in Muong Nong-type tektites from South China. Panels (a, b, e, f) are taken under reflected light, and the rest were taken under transmitted light. Yellow arrows point to the Fe-S spherules and white arrows point to bubbles in the tektites.

Most of our samples and various AASF tektites measured by earlier studies yielded REM values in the normal range of the geomagnetic field (0.005–0.05; Wasilewski & Dickinson, 2000). Figure 14d shows the comparison. Several of the Muong Nong-type tektites from South China exhibit REM > 0.1. Such abnormally large paleointensity also occurs in several Muong Nong-type tektites from Laos and Thailand (Figure 14d), and the larger magnetic field was interpreted to be caused by lightning after the formation of the tektites (Gattacceca et al., 2021). However, splash-form tektites from both South China and the rest of the strewn field do not exhibit REM > 0.1. Meanwhile, 30% of our splash-form tektites and two Muong Nong-type tektites measured by Gattacceca et al. (2021) exhibit REM < 0.005 (Figure 14d), indicating that their recorded paleointensity is less than the geomagnetic field.

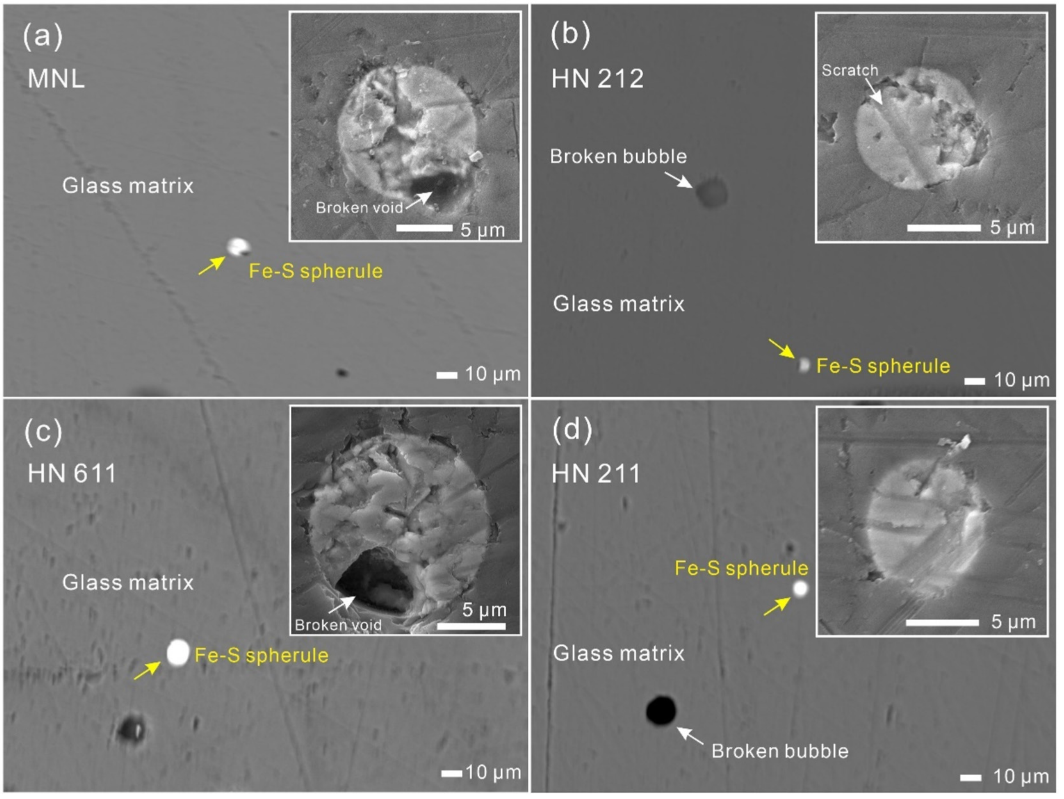

Figure 13. Backscattered electron image for the Fe-S spherules (yellow arrows) in Muong Nong-type tektites from South China. The inserted figures show the high-resolution morphology of the spherules.

4.2. Potential Causes for the Heterogeneous Magnetic Properties of AASF Tektites

Our measurements and comparisons with earlier results show that the magnetic properties of various forms of AASF tektites are dominated by strong paramagnetic signals, while splash-form and ablated splash-form tektites may contain trace amounts of SD magnetite and Muong Nong-type tektites additionally contain small amounts of PSD magnetite. The different magnetic properties of AASF tektites are controlled by the intrinsic properties of magnetic components, for example, concentrations, compositions, and size distributions. Unlike the earlier-advocated positive correlation between FeO content and magnetic susceptibility of tektites in different Cenozoic strewn fields (Rochette et al., 2015), AASF tektites at South China exhibit intermediate contents of FeO and ferromagnetic elements (e.g., Ni, Co; Figure 15) but the lowest magnetic susceptibility (Figure 14a). This comparison indicates that the content of FeO and other magnetic elements in AASF tektites is not the dominant control on their magnetic susceptibility (Figure 14a) or primary remanent magnetization (Figures 14c and 14d).

4.2.1. Possible Effect of Heterogeneous Formation Conditions of Tektite Melts

The magnetic properties of iron-bearing silicate glasses that were formed by rapid cooling are typically dominated by paramagnetic materials (Dunlop & Özdemir, 1997; Nayak et al., 2018; Rochette et al., 2015). This is consistent with the observation that Fe in various tektites is dominated by Fe^{2+} ions (Costa et al., 2014; Koeberl, 1992; Schreiber et al., 1984; Thorpe & Senftle, 1964), and the strong paramagnetic signal of all kinds of AASF tektites is believed to be mainly caused by dispersed Fe^{2+} ions in the glass (Gattacceca et al., 2021; Rochette et al., 2015, 2019). Formation of tektite melts mainly occurred in an extreme-reduced environment, during rapid cooling, Fe atoms in the melt were mostly frozen with a random atomic pattern before crystallization could occur (Spaepen & Turnbull, 1984). The more reduced formation condition of splash-form tektite melt is consistent with the larger average magnetic susceptibility (Figure 14a). Considering that tektites from South China generally exhibit lower magnetic susceptibility than those from the rest of the strewn field, tektite melt ejected toward the uprange of the impactor trajectory may be formed in a less reduced environment. Moreover,

Table 3
Chemical Composition of Fe-S Spherules in the Muong Nong-Type Tektites at South China

Normalized wt%										
Sample	Position	Fe	S	Ti	P	Ni	Co	Cr	Mg	Total
MNL	1	61.57	37.07	0.08	b.d.l.	0.86	0.21	0.07	0.14	100.00
	2	59.63	38.46	0.09	b.d.l.	1.27	0.21	0.08	0.27	100.00
HN211	1	57.78	36.54	0.21	b.d.l.	4.39	0.36	0.07	0.65	100.00
	2	57.68	37.26	0.10	b.d.l.	4.19	0.39	0.10	0.27	100.00
HN212	1	60.68	36.44	0.21	0.02	1.92	0.26	0.07	0.40	100.00
	2	60.06	37.44	0.08	b.d.l.	1.99	0.27	0.06	0.11	100.00
	3	60.69	36.10	0.29	0.04	1.99	0.20	0.07	0.61	100.00
	4	60.39	37.08	0.12	b.d.l.	1.92	0.21	0.08	0.20	100.00
HN611-2	1	61.50	37.09	0.08	b.d.l.	0.93	0.25	0.08	0.07	100.00
HN613	1	56.22	33.06	0.65	b.d.l.	7.64	0.47	0.09	1.85	100.00
Normalized at%										
Sample	Position	Fe	S	Ti	P	Ni	Co	Cr	Mg	Total
MNL	1	0.48	0.51	b.d.l.	b.d.l.	0.01	b.d.l.	b.d.l.	b.d.l.	100.00
	2	0.46	0.52	b.d.l.	b.d.l.	0.01	b.d.l.	b.d.l.	b.d.l.	100.00
HN211	1	0.45	0.50	b.d.l.	b.d.l.	0.03	b.d.l.	b.d.l.	0.01	100.00
	2	0.45	0.51	b.d.l.	b.d.l.	0.03	b.d.l.	b.d.l.	b.d.l.	100.00
HN212	1	0.48	0.50	b.d.l.	b.d.l.	0.01	b.d.l.	b.d.l.	0.01	100.00
	2	0.47	0.51	b.d.l.	b.d.l.	0.01	b.d.l.	b.d.l.	b.d.l.	100.00
	3	0.48	0.49	b.d.l.	b.d.l.	0.01	b.d.l.	b.d.l.	0.01	100.00
	4	0.47	0.51	b.d.l.	b.d.l.	0.01	b.d.l.	b.d.l.	b.d.l.	100.00
HN611-2	1	0.48	0.51	b.d.l.	b.d.l.	0.01	b.d.l.	b.d.l.	b.d.l.	100.00
HN613	1	0.44	0.45	0.01	b.d.l.	0.06	b.d.l.	b.d.l.	0.03	100.00

Note. The b.d.l. is the abbreviation for below detection limit. Note that the element totals of almost all our measurements were below 98 wt% or above 102 wt%, and we neglected the other elements that were not detected and then normalized the analytical data to 100%. Similar procedure performed for such metallic spherules found in impact glass formed by the Bosumtwi crater and Muong Nong-type tektites in southern Laos (El Goresy, 1966; Krizova et al., 2019), and the imperfect measurements were caused by the small sizes of such spherules, as the background glass was unavoidably sensed by the penetrating electron beam (El Goresy, 1966; Krizova et al., 2019).

each morphological type of tektites in the same geographic area exhibits large value range of magnetic susceptibility (Figure 14a), indicating that tektite melt landed at the same area may have experienced different redox states during formation.

Relict mineral shards (e.g., zircon, rutile, monazite) have been observed in various forms of AASF tektites (Folco, Perchiazzi, et al., 2010), especially Muong Nong-type tektites that generally experienced lower shock temperature (Glass & Barlow, 1979; Glass et al., 2020). Our petrographic study for Muong Nong-type tektites from South China yielded relict quartz (Figure 11) but no relict ferromagnetic grains. Meanwhile, un-melted micro-sized chromite (75 μm) was discovered in Muong Nong-type tektites from Indochina, which were likely inherited from the pre-impact target materials (Glass, 1970). The larger M_{rs} and NRM of Muong Nong-type tektites may indicate that they may contain more relicts of ferromagnetic materials (e.g., PSD magnetite) that were inherited from the pre-impact target. On the contrary, the signal of trace amount of SD magnetite in our splash-form tektites has a less chance of being un-melted magnetite from the pre-impact target, considering that melt of splash-form tektites was once heated to a maximum temperature of ~2200°C (e.g., Macris et al., 2018), under which magnetite would experience complete thermal decomposition (Friedman et al., 1960; Senftle & Thorpe, 1959).

10.1029/2022JB025269

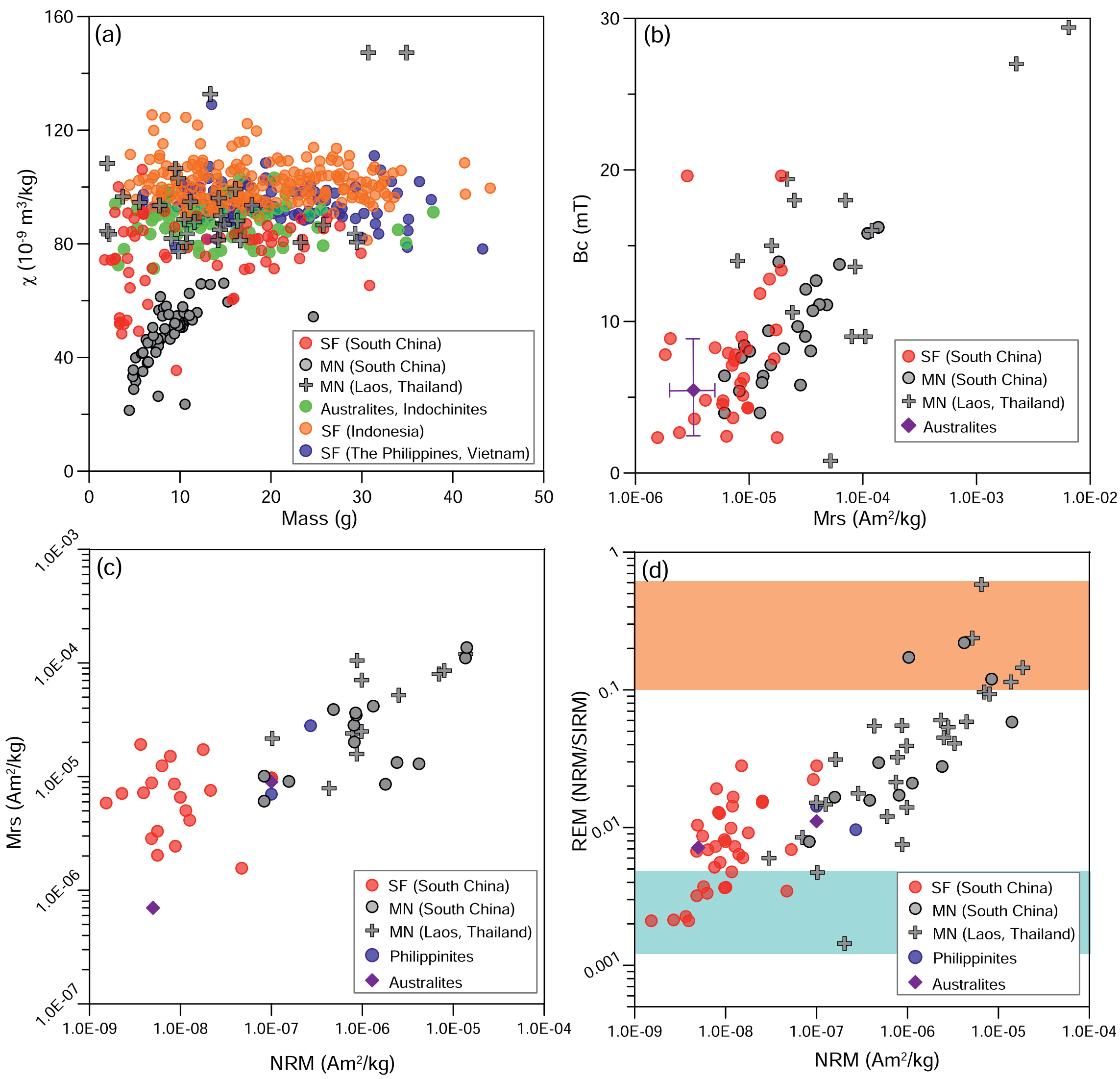

Figure 14. Comparisons of magnetic properties for AASF tektites at different areas. SF = splash-form tektites, MN = Muong Nong-type tektites. (a) Magnetic susceptibility versus mass data. Data reported by Rochette et al. (2019) are referred here. (b) M_{rs} versus B_c. (c) NRM versus M_{rs}. Note that two Muong Nong-type tektites samples reported by Gattacceca et al. (2021) have exceptionally large NRM values, and the two data points are not shown in this panel. (d) The NRM/SIRM ratio versus NRM. Magnetic data of philippinites, australites and Muong Nong-type indochinites are referred from de Gasparis et al. (1975), Donofrio (1977) and Gattacceca et al. (2021). Orange band represents a region of REM > 0.1. Cyan band represents a region of REM < 0.005. Note that panel (d) contains a larger number of samples from South China than panel (c), because the M_{rs} of a portion of samples shown in panel (d) was measured.

4.2.2. Possible Effect of Cooling History of Tektite Melts

While the heterogeneous magnetic properties of AASF tektites can be explained by their different formation conditions (e.g., redox state; Section 4.2.1), different cooling histories (e.g., cooling rate and time) of tektite melts may also explain their observed magnetic properties. The strong effect of cooling rate on magnetic properties of silicate melt was resolved in other impact glasses and volcanic glasses (Carlut & Kent, 2002; Ostertag et al., 1969; Rochette et al., 2015; Schlinger et al., 1988; Schlinger & Smith, 1986). For example, larger impact glasses formed by the Lonar crater experienced lower cooling rate and longer cooling times than smaller ones, and more ferromagnetic materials may grow in the larger glasses, explaining their larger NRM (Weiss et al., 2010). The more rapid cooling of splash-form tektite melt (Wilding et al., 1996) may have suppressed the nucleation and growth of Fe^{2+} ions to form magnetite or other ferromagnetic minerals (Rochette et al., 2015; Senftle & Thorpe, 1959; Werner & Borradaile, 1998). On the contrary, the smaller cooling rate and longer cooling time of Muong Nong-type tektite melts (de Gasparis et al., 1975; Futrell, 1986; Klein et al., 1980) may permit more Fe^{2+} in the melt to form larger grains of ferromagnetic materials (de Gasparis, 1973; Thorpe & Senftle, 1964), such as

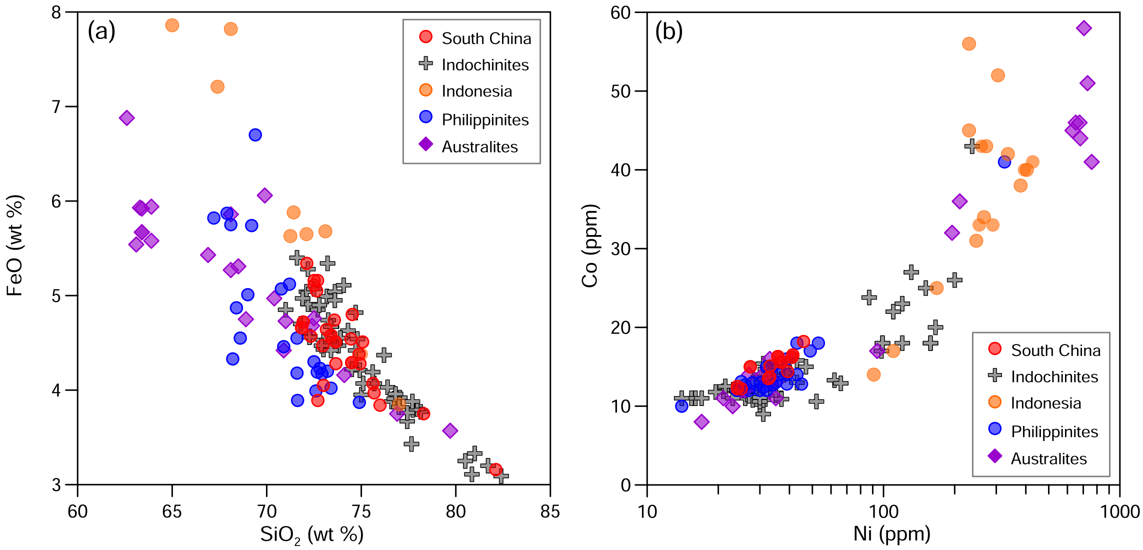

Figure 15. Comparisons of contents of magnetic elements in AASF tektites from different areas. (a) SiO_2 versus FeO. (b) Ni versus Co. Major and trace elements data are referred from Chapman and Scheiber (1969), Ho and Chen (1996), Lee et al. (2004), Goderis et al. (2017), and Ackerman et al. (2019).

SD and PSD magnetite. Assuming that melt of both Muong Nong-type and splash-form AASF tektites contained similar initial amounts of Fe^{2+}, their different cooling histories may yield lower concentration of dispersed Fe^{2+} ions but higher contents of relatively large ferromagnetic grains (e.g., SD and PSD magnetite) in the Muong Nong-type tektites. This interpretation is consistent with the observed magnetic properties of different types of AASF tektites, for example, Muong Nong-type tektites generally have smaller magnetic susceptibility but larger M_{rs} and NRM.

The above interpretation, however, may indicate that SP grains should exist in both the Muong Nong-type and splash-form tektites, if the detected SD and PSD magnetite was grown from smaller grains (de Gasparis, 1973). Although not conclusive, several of our measurement results are consistent with the existence of SP grains in both the Muong Nong-type and splash-form tektites: (a) the relatively erratic IRM acquisition curves of the splash-form tektites (Figures 5d–5f) are consistent with being caused by thermal relaxation of SP grains in low-magnetization materials (Lanci & Kent, 2006); (b) FORC diagrams have relatively small noises at low fields, and strong signals of thermal relaxation are visible along the B_u axis, that is, B_c close to 0 (Figures S5 and S6 in Supporting Information S1), consistent with the possible existence of trace amounts of SP particles (Pike et al., 2001; Roberts et al., 2000); (c) the low-temperature magnetic behavior of our samples (Figures 8 and 9) exhibits sharp increases from about 90 to 10 K, which can be explained by both the dominating paramagnetic signals and trace amounts of SP grains (Moskowitz et al., 1989; Nayak et al., 2018; Starunov et al., 2019).

4.2.3. Possible Effect of Motional Magnetization of Tektite Melts

It is a consensus that Muong Nong-type tektites are located closer to the source crater than the other AASF tektites, and they may be landed with a high temperature, possible above the blocking temperature of magnetic carriers (de Gasparis et al., 1975; Gattacceca et al., 2021). On the contrary, most splash-form tektites were likely entrained in an upward and outward expanding hot impact plume for a longer time than Muong Nong-type tektites (Howard, 2011; Jones & John, 1982; Koeberl, 1994; Melosh, 1990). During the dissipation of the impact plume toward high altitude and downrange of the impact trajectory, centimeter-sized molten tektites were quenched within a couple of minutes (Artemieva, 2008a; Macris et al., 2018), while their orientation may have undergone frequent changes due to rolling and tumbling with respect to the geomagnetic field, recording unstable magnetization directions and thus weaker NRM (Weiss et al., 2010). Therefore, motional magnetization likely occurred during the cooling of tektite melt, especially that of the splash-form tektites. This interpretation explains the larger NRM and REM of Muong Nong-type tektites than those of the splash-form tektites, and tektite melt with relative fast rotation during quenching may record REM less than the normal range of geomagnetic field, that is, samples in the cyan shade of Figure 14d. This mechanism was also referred to explain the stable NRM demagnetization behaviors of the Muong Nong-type tektites from Laos and Thailand (Gattacceca et al., 2021).

The REM values of most AASF tektites, including our samples and cores of philippinites and australites, are within the normal range of geomagnetic field (Figure 14d). If motional magnetization occurred during the cooling of these tektite melts, their orientations with respect to the local geomagnetic field might have been relatively stable when passing the blocking temperature of magnetic carriers (e.g., SD and PSD magnetite). This interpretation is consistent with earlier interpretations that many Muong Nong-type tektites from Laos and Thailand may be cooled below the blocking temperature of magnetite after landing on the surface (Gattacceca et al., 2021). Earlier field investigations suggested that Muong Nong-type tektites from Thailand may be landed with a plastic state in terms of the mechanical properties (Fiske et al., 1999). Recent field studies for fragments of Muong Nong-type tektites at Thailand suggested in situ intensive fragmentation upon landing, indicating that the Muong Nong-type tektites had a brittle mechanical behavior when landed (Tada et al., 2020). It was also observed that splash-form tektites at Vietnam had a brittle skin and plastic interior when landed (Nininger & Huss, 1967). The liquid to solid transition temperature of tektite melt is about 780°C (Wilding et al., 1996). Therefore, tektites with REM $\approx$ 0.005–0.1 may be landed with a temperature less than 780°C but larger than the blocking temperature of magnetic carriers (e.g., 580°C for magnetite).

While post-landing acquisition of NRM might be plausible for most tektites at South China and the Indochina Peninsula, which are close to the hypothesized source crater at Indochina, the melt of australites was cooled before the atmospheric reentry (Chapman, 1971). Cores of australites exhibit comparable REM with normal geomagnetic field (Figure 14d), indicating that during the ascending of melt of australites (possibly in the expanding impact plume; Elkins-tanton et al., 2003; Magna et al., 2011), the orientation of the melt may be relatively stable when cooled through the blocking temperature of the interior magnetic carriers. Follow this interpretation, it is alternatively possible that other tektites that have comparable REM with normal geomagnetic field may also be cooled below the Curie temperature during flight with relatively stable orientations, and their different NRM and REM values may record an altitude dependence of geomagnetic field intensity (Donofrio, 1977).

4.2.4. Possible Origin of Abnormally Large Magnetic Field Recorded by Tektites

While the abnormally low REM of several splash-form tektites from South China and a few Muong Nong-type tektites from Laos and Thailand ($<$0.005; Figure 14d) can be interpreted by rapid reorientation during cooling (i.e., motional magnetization) and/or cooling at rather high altitudes, several Muong Nong-type tektites from both South China, Laos and Thailand (Gattacceca et al., 2021) exhibit REM $>$ 0.1 (orange shade of Figure 14d). These samples record abnormally strong magnetic field compared with the geomagnetic field (Gattacceca et al., 2021). Random post-deposition events, such as lightning remagnetization and exposure to hand magnets, were invoked to explain the abnormally large REM (Gattacceca et al., 2021; Gattacceca & Rochette, 2004; Wasilewski & Dickinson, 2000). While our samples were not exposed to strong artificial magnetic fields before laboratory measurement, lightning remagnetization is hard to reconcile the observation that all the splash-form tektites from South China have REM $\ll$ 0.1.

Impact-generated magnetic fields were frequently induced to explain the origin of patches of abnormally strong magnetic areas on the Moon (Crawford, 2020; Crawford & Schultz, 1988, 1999; Hood & Artemieva, 2008). Such induced magnetic fields are supposed to be formed by ejection of negatively-charged impact debris and retainment of positively-charged plasma above the impact site (Crawford & Schultz, 1999). Analytical models for impact-generated plasma and magnetic field predicted that for terrestrial impacts, a 1 km diameter projectile could generate a transient magnetic field that is up to 0.03 T and could last $\sim$100 s, and dust discharge would tend to reduce both the intensity and lifetime of the induced magnetic field with time (Crawford & Schultz, 1999). However, evidence for impact-generated magnetic field on Earth has been scarce (Carporzen et al., 2012; Louzada et al., 2008; Weiss et al., 2010). Our observations are not adequate to postulate whether or not a hypothesized impact-induced magnetic field could cause the abnormally large REM values recorded by the Muong Nong-type tektites. This scenario, if true, would be highly informative to resolving the fine structure of impact-induced magnetic fields based on magnetic properties of tektites.

In summary, we propose the following potential causes for the observed heterogeneous magnetic properties of AASF tektites, which are mainly related with the different formation condition and cooling history of tektite melts: (a) the faster cooling rate and more reduced cooling environment of splash-form tektite melt may be able to form a larger portion of dispersed Fe^{2+} ions in splash-form tektites, explaining the larger average magnetic susceptibility of the splash-form tektites; (b) on average, splash-form tektites have higher shock level (e.g., heating temperature) and larger cooling rates than Muong Nong-type tektites, so large grains of magnetite (PSD magnetite) may exist in the Muong Nong-type tektites than those in the splash-form tektites; (c) most tektites might have relatively stable orientation in the geomagnetic field when cooled below the blocking temperature, and motional magnetization and/or cooling at rather high altitudes may cause ratios of equivalent magnetization less than that of geomagnetic field; (d) abnormally strong magnetic field(s) might exist during and/or after the formation of some Muong Nong-type tektites, but a potential causal correlation with impact-induced magnetic field and/or post-deposition lightning is obscure.

4.3. Origin of Fe-S Spherules in Muong Nong-Type Tektites From South China

We report the first identification of Fe-S spherules in AASF tektites at South China (Figures 11–13). Ferromagnetic inclusions in AASF tektites at the Indochina Peninsula and further south have been extensively searched and studied (de Gasparis, 1973; Donofrio, 1977; Kleinmann, 1969; Rochette et al., 2015, 2019). Chao et al. (1962, 1964) discovered metallic spherules in some philippinites and indochinites, which consist of kamacite, troilite and schreibersite. Senftle et al. (1964) referred to this observation and suggested that the detected significant signals of ferromagnetic materials in some philippinites were likely caused by submicroscopic metallic-iron spherules within the glass. However, such spherules were not observed in microscopes. Kleinmann (1969) observed finely distributed magnetite skeletons and idiomorphic magnetite crystals in indochinites, suggesting that they were formed by rapid crystallization in the high-temperature melt. To determine the stable remanence carrier in AASF tektites, Donofrio (1977) observed some MD iron-nickel particles in several philippinites, which were not regarded as reliable carrier for NRM considering their lower coercivity. Recently, Gattacceca et al. (2021) confirmed the presence of signals of PSD magnetite and MD metallic iron in Muong Nong-type tektites from southern Laos and northeastern Thailand based on rock magnetic analyses.

At present, the source of metallic particles discovered in AASF tektites remains controversial. Melting of impactor components such as troilite-pentlandite-like phases were preferred as the origin of the Fe-Ni sulfides and other metallic spherules (e.g., iron-nickel and iron phosphide particles) in different types of AASF tektites (Chao et al., 1962, 1964; Donofrio, 1977; Kleinmann, 1969). On the other hand, contents of highly siderophile elements (e.g., Ni, Co, Cr) in tektites exhibit large regional variations across AASF, in which Muong Nong-type tektites from South China contain relatively low Ni (below 60 ppm; Goderis et al., 2017), Co (~11 ppm), and Cr (~72 ppm) (Chapman & Scheiber, 1969). Metallic spherules found in philippinites exhibited similar Fe/Ni and Ni/Co ratios with terrestrial rocks, and impact-induced in situ reduction of pre-impact target was proposed as a plausible explanation (Ganapathy & Larimer, 1983). Likewise, the Fe-Ni sulfide particles in the Muong Nong-type tektites from Laos were interpreted to be formed by melting of unstable sulfides in the pre-impact target (Krizova et al., 2019).

Relict magnetic minerals (such as magnetite and hematite) have been found in impact glasses (not tektites) formed by the Ries (Kleinmann, 1969), Bosumtwi (El Goresy, 1966), and Zhamanshin craters (Starunov et al., 2019), and also in glass formed by the 1908 Tunguska air blast (Kirova, 1964). With large sizes (up to hundreds of μm) and broken angular shapes, such magnetic inclusions showed evidence of relatively low degree of shock metamorphism (Glass & Barlow, 1979; Starunov et al., 2019). For comparison, the Fe-S spherules in the Muong Nong-type tektites from South China exhibit sharp circular boundaries with the surrounding glass (Figures 12 and 13), indicating immiscibility between the Fe-S metallic melt and silicate melt during rapid cooling (Belkin & Horton, 2009; Hamann et al., 2017; Reid et al., 1964). Therefore, the Fe-S spherules in the Muong Nong-type tektites from South China are not un-melted relict particles from the target and/or impactor materials.

Our EPMA measurements for the Fe-S spherules reveal that the average Fe/S ratio (0.94; Table 3) is close to that of stoichiometric FeS (troilite; FeS) but different with that of pyrite (FeS_2; 0.5) and greigite (Fe_3S_4; 0.75). The RT-SIRM behavior at ~10–90 K (Figure 8) of the Muong Nong-type tektites at South China is similar with that of antiferromagnetic iron sulfides, such as troilite (Cuda et al., 2011; Kohout et al., 2007, 2010). However, the low-temperature magnetic behavior of Muong Nong-type tektites from South China (Figure 8) exhibits no magnetic transition at ~34 K that is caused by monoclinic pyrrhotite (Fe_7S_8; Rochette et al., 1990) or at ~70 K that is caused by troilite (Cuda et al., 2011). Therefore, both the compositions of the Fe-S spherules and the low-temperature magnetic properties of the host tektites indicate that the discovered Fe-S spherules are not likely troilite or monoclinic pyrrhotite.

The Ni content of the Fe-S spherules in the Muong Nong-type tektites from South China (average value of about 2.71 wt%) is much lower than that of the Fe-Ni-S particles in the Muong Nong-type tektites from Laos (~32–39 wt%), which were interpreted to have an impactor origin (Krizova et al., 2019). In addition, the average Ni/Co ratio of the Fe-S spherules (~9; Table 3) is similar with that of typical terrestrial materials (5–10; Ganapathy

& Larimer, 1983), but it is different from that of typical Fe-S minerals in meteorites (larger than 20), such as troilite (FeS; Nichiporuk & Chodos, 1959; Allen & Mason, 1973), Shengzhuangite ($NiFeS_2$; Bindi & Xie, 2018), and Pentlandite ($(Fe, Ni)_9S_8$; Olsen et al., 1999). Therefore, the Fe-S spherules are most likely originated from iron-sulfides in the pre-impact target materials instead of from the impactor.

The precise composition and interior structure of the Fe-S spherules are not resolved yet, and their possible contributions to the observed magnetic properties of the host Muong Nong-type tektites are not known. Although several such Fe-S spherules are resolved in a small piece of Muong Nong-type tektite that has relatively strong signals of PSD particles (Section 3.3), the occurrence frequency of such spherules in the other Muong Nong-type tektites is uncertain. Based on the current available data of these spherules and their host tektites, our preferred interpretation, that their precursor being pre-impact target materials, does not yield additional insights into the possible location of the parent crater.

4.4. Limitations and Prospection

Our rock magnetic results for the tektites from South China are generally consistent with earlier studies for AASF tektites from the other areas (de Gasparis, 1973; de Gasparis et al., 1975; Donofrio, 1977; Gattacceca et al., 2021; Rochette et al., 2015). The cross comparisons (Sections 4.1 and 4.2) yielded larger heterogenies in the magnetic properties of the tektites than earlier findings, providing additional insight into the formation of tektites. However, many magnetic signals of the tektites are still ambiguous based on our current knowledge of rock magnetism. Due to the extremely weak magnetization, AASF tektites, especially the splash-form tektites, are not ideal samples to extract ferromagnetic signals (de Gasparis, 1973; Donofrio, 1977; Rochette et al., 2015; Werner & Borradaile, 1998). Therefore, both the FORC diagrams and temperature dependence of magnetic susceptibility obtained at high-temperature exhibit large noises, which do not show distinct evidence of known magnetic particles (Figures S5, S6, and S7 in Supporting Information S1). Although our data can be explained by a trace amount of SP particles in both the splash-form and Muong Nong-type tektites, conclusive evidence awaits further measurements, for example, more systematic low-temperature rock magnetism study. The abnormally large REM of several Muong Nong-type tektites from South China and Indochina needs verification based on more accurate measurements for the absolute paleointensity and paleomagnetism. Afterward, the possible origin(s) of the indicated strong magnetic field(s) can be better resolved by integrating theoretical calculations for the spatial distribution of impact-induced magnetic field and the cooling history and flight trajectory of various tektite melts.

As a new discovery, the Fe-S spherules in the Muong Nong-type tektites from South China deserve systematic investigations for their precise composition, high-resolution crystallography, and magnetic properties. Afterward, their implications to the possible lithology and depositional environment of the precursor target materials can be anticipated.

5. Conclusions

The first detailed rock magnetism investigation is carried out for Australasian tektites from South China in this study. Their magnetic properties are compared with those of various morphological types of tektites (Muong Nong-type and splash-form) from the other places of this strewn field. We confirm that the magnetic properties of AASF tektites from both South China and elsewhere are dominated by paramagnetic signals. While trace amounts of superparamagnetic grains may exist in the tektites from South China, we find signals caused by small amounts of single-domain magnetite in the splash-form tektites and PSD magnetite may exist in the Muong Nong-type tektites.

We reveal that each morphological type of tektites from a same geographic area exhibits large variations of magnetic properties. In general, the average magnetic susceptibility of tektites from South China is lower than that of the other AASF tektites, and that of the Muong Nong-type tektites from South China is the lowest in the entire strewn field. The average natural remanent magnetization and average ratio of equivalent magnetization of splash-form tektites from South China are the lowest in the strewn field, while they are comparable with those of few reported values for australites. These heterogeneous magnetic properties can be explained by the different shock levels and/or cooling history of the tektite melts, as the Muong Nong-type tektites might contain more relicts of magnetic carriers from the precursor materials, and/or a slower cooling rate and longer cooling time of Muong Nong-type tektites may cause higher abundances and larger grain sizes of ferromagnetic minerals.

Most AASF tektites, including the splash-form tektites from South China and australites, have ratios of equivalent magnetization comparable with the range of normal geomagnetic field. These tektite melts might have a relatively stable orientation with respect to the geomagnetic field when cooled through the blocking temperature of the magnetic carriers. Some of the tektites might be cooled through the Curie point after landing. A portion of splash-form tektites and few earlier reported Muong Nong-type tektites from the Indochina Peninsula record much lower ratios of equivalent magnetization less than that of geomagnetic field, which can be explained by motional magnetization of rapidly rotating tektite melt during cooling and/or cooling at high altitudes. No splash-form tektites but several Muong Nong-type tektites from South China and Indochina Peninsula exhibit abnormally large ratios of equivalent magnetization, but the origin of strong magnetic field(s) during and/after the formation of these tektites is unknown. We suggest that the above interpretations are informative to the understanding of the impact process that formed the enigmatic source crater.

This study also reports the first discovery of micro-sized Fe-S spherules in the Muong Nong-type tektites from South China. Their morphology and composition indicate that they were formed due to immiscibility between Fe-S metallic melt and silicate melt during cooling. While their precise geochemistry, interior structure, and possible contribution to the magnetic properties of the host tektites are not resolved yet, preliminary compositional analyses suggest that the spherules are likely originated from the pre-impact target materials.

This study demonstrates the usefulness of rock magnetism, especially its combination with detailed petrographic observations, in studying the origin of AASF tektites.

Data Availability Statement

All raw data collected in this manuscript can be accessible through the zenodo data repository (https://doi.org/10.5281/zenodo.7690063) and figshare data repository (https://doi.org/10.6084/m9.figshare.21608103.v4).

Acknowledgments

This study is supported by the National Natural Science Foundation of China (42241108, 42273040, 42003053) and the Strategic Priority Research Program of Chinese Academy of Science (XDB41000000). The authors are grateful to Dr. Zongmin ZHU, Huiru XU, Yingchao XU, Yanxue WU, Zhiyu YI, Tingwei ZHANG, Xiaoqiang YANG, Xiaodong TAN, Huafeng QIN, and Ms. Suping WU, Yulin HAN, Meiling ZHOU for laboratory assistance. Mr. Haosheng ZHONG from Maoming, Guangdong Province provided some additional MN type tektites. Mr. Jiang PU, Yichen WANG, Shaopeng XU, Yizhen MA, Wenbin SHI, and Miss Yuelu CHEN joined the field trips. Comments provided by the editor and two anonymous reviewers are constructive that have helped to improve the manuscript.

References

Ackerman, L., Skala, R., Krizova, S., Zak, K., & Magna, T. (2019). The quest for an extraterrestrial component in Muong Nong-type and splash-form Australasian tektites from Laos using highly siderophile elements and Re-Os isotope systematics. *Geochimica et Cosmochimica Acta*, *252*, 179–189. https://doi.org/10.1016/j.gca.2019.03.009

Ackerman, L., Zak, K., Skala, R., Rejsek, J., Krizova, S., Wimpenny, J., & Magna, T. (2020). Sr-Nd-Pb isotope systematics of Australasian tektites: Implications for the nature and composition of target materials and possible volatile loss of Pb. *Geochimica et Cosmochimica Acta*, *276*, 135–150. https://doi.org/10.1016/j.gca.2020.02.025

Albin, E. F., Norman, M. D., & Roden, M. (2000). Major and trace element compositions of georgiaites: Clues to the source of North American tektites. *Meteoritics & Planetary Sciences*, *35*(4), 795–806. https://doi.org/10.1111/j.1945-5100.2000.tb01463.x

Allen, R. O. J., & Mason, B. (1973). Minor and trace elements in some meteoritic minerals. *Geochimica et Cosmochimica Acta*, *37*(6), 1435–1456. https://doi.org/10.1016/0016-7037(73)90081-1

Amare, K., & Koeberl, C. (2006). Variation of chemical composition in Australasian tektites from different localities in Vietnam. *Meteoritics & Planetary Sciences*, *41*(1), 107–123. https://doi.org/10.1111/j.1945-5100.2006.tb00196.x

Artemieva, N. (2008a). Tektites: Model versus reality. *Lunar and Planetary Science*, *XXXIX*, 1651.

Artemieva, N. A. (2008b). High-velocity impact ejecta: Tektite and Martian meteorites. In V. V. Adushkin & I. V. Nemchinov (Eds.), *Catastrophic events caused by cosmic objects* (1nd ed., pp. 267–289). Springer.

Artemieva, N. A. (2013). Numerical modeling of the Australasian strewn field. In *Proceeding of the forty-fourth lunar and planetary science conference* (p. 1410).

Aubourg, C., & Pozzi, J. P. (2010). Toward a new <250°C pyrrhotite–magnetite geothermometer for claystones. *Earth and Planetary Science Letters*, *294*(1–2), 47–57. https://doi.org/10.1016/j.epsl.2010.02.045

Baldwin, K. A., Butler, S. L., & Hill, R. J. (2015). Artificial tektites: An experimental technique for capturing the shapes of spinning drops. *Scientific Reports*, *5*(1), 7660. https://doi.org/10.1038/srep07660

Barnes, V. E. (1969). Progress of tektite studies in China. *Eos*, *50*(12), 704–709. https://doi.org/10.1029/eo050i012p00704

Barnes, V. E., & Pitakpaivan, K. (1962). Origin of indochinite tektites. *Proceedings of the National Academy of Sciences of the United States of America*, *48*(6), 947–955. https://doi.org/10.1073/pnas.48.6.947

Belkin, H. E., & Horton, J. W., Jr. (2009). Silicate glasses and sulfide melts in the ICDP-USGS Eyreville B core, Chesapeake Bay impact structure, Virginia, USA. In G. S. Gohn, C. Koeberl, K. G. Miller, & W. U. Reimold (Eds.), *The ICDP-USGS deep drilling project in the Chesapeake Bay impact structure: Results from the Eyreville core holes* (Vol. 458, pp. 447–468). *Geological Society of America Special Paper*.

Bindi, L., & Xie, X. (2018). Shenzhuangite, NiFeS2, the Ni-analogue of chalcopyrite from the Suizhou L6 chondrite. *European Journal of Mineralogy*, *30*(1), 1–5. https://doi.org/10.1127/ejm/2017/0029-2684

Blum, D. J., Papanastassiou, D. A., Koeberl, C., & Wasserburg, G. J. (1992). Neodymium and strontium isotopic study of Australasian tektites: New constraints on the provenance and age of target materials. *Geochimica et Cosmochimica Acta*, *56*(1), 483–492. https://doi.org/10.1016/0016-7037(92)90146-a

Carlut, J., & Kent, D. V. (2002). Grain-size-dependent paleointensity results from very recent mid-oceanic ridge basalts. *Journal of Geophysical Research*, *107*(B3), 2049. https://doi.org/10.1029/2001JB000439

Carporzen, L., Weiss, B. P., Gilder, S. A., Pommier, A., & Hart, R. J. (2012). Lightning remagnetization of the Vredefort impact crater: No evidence for impact-generated magnetic fields. *Journal of Geophysical Research*, *117*(E1), E01007. https://doi.org/10.1029/2011JE003919

Cavosie, A. J., Timms, N. E., Erickson, T. M., & Koeberl, C. (2018). New clues from Earth's most elusive impact crater: Evidence of reidite in Australasian tektites from Thailand. *Geology*, *46*(3), 203–206. https://doi.org/10.1130/G39711.1

Chao, E. C. T., Adler, I., Dwornik, E. J., & Littler, J. (1962). Metallic spherules in tektites from Isabela, Philippine Islands. *Science*, *135*(3498), 97–98. https://doi.org/10.1126/science.135.3498.97

Chao, E. C. T., Dwornik, E. J., & Littler, J. (1964). New data on the nickel-iron spherufes from Southeast Asian tektites and their implications. *Geochimica et Cosmochimica Acta*, *28*(6), 971–980. https://doi.org/10.1016/0016-7037(64)90044-4

Chapman, D. R. (1971). Australasian tektite geographic pattern, crater and ray of origin, and theory of tektite events. *Journal of Geophysical Research*, *76*(26), 6309–6338. https://doi.org/10.1029/JB076i026p06309

Chapman, D. R., & Scheiber, L. C. (1969). Chemical investigation of Australasian tektites. *Journal of Geophysical Research*, *74*(27), 6737–6776. https://doi.org/10.1029/JB074i027p06737

Chaussidon, M., & Koeberl, C. (1995). Boron content and isotopic composition of tektites and impact glasses; constraints on source regions. *Geochimica et Cosmochimica Acta*, *59*(3), 613–624. https://doi.org/10.1016/0016-7037(94)00368-V

Church, N., Feinberg, J. M., & Harrison, R. (2011). Low-temperature domain wall pinning in titanomagnetite Quantitative modeling of multidomain first-order reversal curve diagrams and AC susceptibility. *Geochemistry, Geophysics, Geosystems*, *12*(7), Q07Z27. https://doi.org/10.1029/2011GC003538

Cisowski, S. M., Fuller, M. D., Wu, Y. M., Rose, M. F., & Wasilewski, P. J. (1975). Magnetic effects of shock and their implications for magnetism of lunar samples. *Proceeding of the sixth Lunar and Planetary Science Conference*(pp. 3123–3141).

Coey, J. M. D., & Ghose, S. (1988). Magnetic phase transitions in silicate minerals. In S. Ghose, J. M. D. Coey, & E. Salje (Eds.), *Structural and magnetic phase transitions in minerals* (1nd ed., pp. 162–184). Springer.

Costa, B. F. O., Klingelhöfer, G., Panthöfer, M., & Alves, F. I. (2014). Backscattering Mossbauer MIMOS II and XRF studies on tektites from different strewn fields. *Hyperfine Interactions*, *226*(1–3), 613–619. https://doi.org/10.1007/s10751-013-0986-3

Crawford, D. A. (2020). Simulations of magnetic fields produced by asteroid impact: Possible implications for planetary paleomagnetism. *International Journal of Impact Engineering*, *137*, 103464. https://doi.org/10.1016/j.ijimpeng.2019.103464

Crawford, D. A., & Schultz, P. H. (1988). Laboratory observations of impact-generated magnetic fields. *Nature*, *336*(6194), 50–52. https://doi.org/10.1038/336050a0

Crawford, D. A., & Schultz, P. H. (1999). Electromagnetic properties of impact-generated plasma, vapor and debris. *International Journal of Impact Engineering*, *23*(1), 169–180. https://doi.org/10.1016/S0734-743X(99)00070-6

Cuda, J., Kohout, T., Tucek, J., Haloda, J., Filip, J., Prucek, R., & Zboril, R. (2011). Low-temperature magnetic transition in troilite: A simple marker for highly stoichiometric FeS systems. *Journal of Geophysical Research*, *116*(B11), B11205. https://doi.org/10.1029/2011jb008232

Cuttitta, F., Carron, M. K., & Annell, C. S. (1972). New data on selected Ivory Coast tektites. *Geochimica et Cosmochimica Acta*, *36*(11), 1297–1309. https://doi.org/10.1016/0016-7037(72)90050-6

Day, R., Fuller, M., & Schmidt, V. A. (1977). Hysteresis properties of titanomagnetite: Grain-size and compositional dependence. *Physics of the Earth and Planetary Interiors*, *13*(4), 260–267. https://doi.org/10.1016/0031-9201(77)90108-X

Dearing, J. A., Dann, R. J. L., Hay, K., Lees, J. A., Loveland, P. J., Maher, B. A., & O'Grady, K. (1996). Frequency-dependent susceptibility measurements of environmental materials. *Geophysical Journal International*, *124*(1), 228–240. https://doi.org/10.1111/j.1365-246X.1996.tb06366.x

de Gasparis, A. A. (1973). *Magnetic properties of tektites and impact glasses*. The University of Pittsburgh.

de Gasparis, A. A., Fuller, M., & Cassidy, W. (1975). Natural remanent magnetism of tektites of the Muong-Nong type and its bearing on models of their origin. *Geology*, *3*(10), 605–607. https://doi.org/10.1130/0091-7613(1975)3<605:NRMOTO>2.0.CO;2

Donofrio, R. R. (1977). *The magnetic environment of the tektites*. The University of Oklahoma.

Dunlop, D. J. (2002). Theory and application of the Day plot (M_{rs}/M_s versus H_{cr}/H_c) 1. Theoretical curves and tests using titanomagnetite data. *Journal of Geophysical Research*, *107*(B3), 2056. https://doi.org/10.1029/2001JB000486

Dunlop, D. J., & Özdemir, Ö. (1997). *Rock magnetism: Fundamentals and frontiers*. Cambridge University Press.

El Goresy, A. (1966). Metallic spherules in Bosumtwi crater glasses. *Earth and Planetary Science Letters*, *1*, 23–24. https://doi.org/10.1016/0012-821X(66)90099-9

Elkins-tanton, L. T., Aussillous, P., Bico, J., Quere, D., & Bush, J. W. M. (2003). A laboratory model of splash-form tektites. *Meteoritics & Planetary Sciences*, *38*(9), 1331–1340. https://doi.org/10.1111/j.1945-5100.2003.tb00317.x

Fiske, P. S., Putthapiban, P., & Wasson, J. T. (1996). Excavation and analysis of layered tektites from northeast Thailand: Results of 1994 field expedition. *Meteoritics & Planetary Sciences*, *31*(1), 36–41. https://doi.org/10.1111/j.1945-5100.1996.tb02050.x

Fiske, P. S., Schnetzler, C. C., Mchone, J., Chanthavaichith, K. K., Homsombath, I., Phouthakayalat, T., et al. (1999). Layered tektites of Southeast Asia: Field studies in central Laos and Vietnam. *Meteoritics & Planetary Sciences*, *34*(5), 757–761. https://doi.org/10.1111/j.1945-5100.1999.tb01388.x

Folco, L., Glass, B. P., D'Orazio, M., & Rochette, P. (2010). A common volatilization trend in Transantarctic Mountain and Australasian microtektites: Implications for their formation model and parent crater location. *Earth and Planetary Science Letters*, *293*(1–2), 135–139. https://doi.org/10.1016/j.epsl.2010.02.037

Folco, L., Perchiazzi, N., D'Orazio, M., Frezzotti, M. L., Glass, B. P., & Rochette, P. (2010). Shocked quartz and other mineral inclusions in Australasian microtektites. *Geology*, *38*(3), 211–214. https://doi.org/10.1130/G30512.1

Friedman, I., Thorpe, A., & Senftle, E. (1960). Comparison of the chemical composition and magnetic properties of tektites and glasses formed by fusion of terrestrial rocks. *Nature*, *187*(4743), 1089–1092. https://doi.org/10.1038/1871089a0

Fuller, M., Cisowski, S., Hart, M., Haston, R., Schmidtke, E., & Jarrard, R. (1988). NRM: IRM(S) demagnetization plots; an aid to the interpretation of natural remanent magnetization. *Geophysical Research Letters*, *15*(5), 518–521. https://doi.org/10.1029/GL015i005p00518

Futrell, D. S. (1986). Implication of welded breccia in Muong Nong-type tektites. *Nature*, *319*(6055), 663–665. https://doi.org/10.1038/319663a0

Futrell, D. S., & Wasson, J. T. (1993). A 10.8-kg layered (Muong Nong-type) tektite from Wenchang, Hainan, China. *Meteoritics*, *28*(1), 136–137. https://doi.org/10.1111/j.1945-5100.1993.tb00259.x

Ganapathy, R., & Larimer, J. W. (1983). Nickel-iron spherules in tektites non-meteoritic in origin. *Earth and Planetary Science Letters*, *65*(2), 225–228. https://doi.org/10.1016/0012-821X(83)90160-7

Gattacceca, J., & Rochette, P. (2004). Toward a robust normalized magnetic paleointensity method applied to meteorites. *Earth and Planetary Science Letters*, *227*(3–4), 377–393. https://doi.org/10.1016/j.epsl.2004.09.013

Gattacceca, J., Rochette, P., Quesnel, Y., Singsoupho, S., & Krot, A. (2021). Revisiting the paleomagnetism of Muong Nong layered tektites: Implications for their formation process. *Meteoritics & Planetary Sciences*, *57*, (2), 1–14. https://doi.org/10.1111/maps.13703

Geiss, C. E., Zanner, C. W., Banerjee, S. K., & Joanna, M. (2004). Signature of magnetic enhancement in a loessic soil in Nebraska, United States of America. *Earth and Planetary Science Letters*, *228*(3–4), 355–367. https://doi.org/10.1016/j.epsl.2004.10.011

Giuli, G., Pratesi, G., Cipriani, C., & Paris, E. (2002). Iron local structure in tektites and impact glasses by extended X-ray absorption fine structure and high-resolution X-ray absorption near-edge structure spectroscopy. *Geochimica et Cosmochimica Acta*, *66*(24), 4347–4353. https://doi.org/10.1016/S0016-7037(02)01030-X

Glass, B., & Heezen, B. C. (1967). Tektites and geomagnetic reversal. *Nature*, *214*(5086), 372. https://doi.org/10.1038/scientificamerican0767-32

Glass, B. P. (1970). Zircon and chromite crystals in a Muong Nong-type tektite. *Science*, *169*(3947), 766–769. https://doi.org/10.1126/science.169.3947.766

Glass, B. P. (1990). Tektites and microtektites: Key facts and inferences. *Tectonophysics*, *171*(1–4), 393–404. https://doi.org/10.1016/0040-1951(90)90112-L

Glass, B. P., & Barlow, R. A. (1979). Mineral inclusions in Muong Nong-type indochinites: Implications concerning parent material and process of formation. *Meteoritics*, *14*(1), 55–67. https://doi.org/10.1111/j.1945-5100.1979.tb00479.x

Glass, B. P., Folco, L., Masotta, M., & Campanale, F. (2020). Coesite in a Muong Nong-type tektite from Muong Phin, Laos: Description, formation, and survival. *Meteoritics & Planetary Sciences*, *55*(3), 253–273. https://doi.org/10.1111/maps.13433

Glass, B. P., & Koeberl, C. (2006). Australasian microtektites and associated impact ejecta in the South China Sea and the middle Pleistocene supereruption of Toba. *Meteoritics & Planetary Sciences*, *41*(2), 305–326. https://doi.org/10.1111/j.1945-5100.2006.tb00211.x

Glass, B. P., & Pizzuto, J. E. (1994). Geographic variation in Australasian microtektite concentrations: Implications concerning the location and size of the source crater. *Journal of Geophysical Research*, *99*(B4), 19075–19081. https://doi.org/10.1029/94JE01866

Glass, B. P., & Simonson, B. M. (2013). *Distal impact ejecta layers: A record of large impacts in sedimentary deposits*. Springer. https://doi.org/10.1007/978-3-540-88262-6

Goderis, S., Tagle, R., Fritz, J., Bartoschewitz, R., & Artemieva, N. (2017). On the nature of the Ni-rich component in splash-form Australasian tektites. *Geochimica et Cosmochimica Acta*, *217*, 28–50. https://doi.org/10.1016/j.gca.2017.08.013

Haines, P. W., Howard, K. T., Ali, J. R., Burrett, C. F., & Bunopas, S. (2004). Flood deposits penecontemporaneous with ~0.8 Ma tektite fall in NE Thailand: Impact-induced environmental effects? *Earth and Planetary Science Letters*, *225*(1–2), 19–28. https://doi.org/10.1016/j.epsl.2004.05.008

Hamann, C., Fazio, A., Ebert, M., Hecht, L., Wirth, R., Folco, L., et al. (2017). Silicate liquid immiscibility in impact melts. *Meteoritics & Planetary Sciences*, *53*(8), 1–39. https://doi.org/10.1111/maps.12907

Harrison, R. J., & Feinberg, J. M. (2008). FORCinel: An improved algorithm for calculating first-order reversal curve distributions using locally weighted regression smoothing. *Geochemistry, Geophysics, Geosystems*, *9*(5), Q05016. https://doi.org/10.1029/2008GC001987

Heslop, D., McIntosh, G., & Dekkers, M. J. (2004). Using time- and temperature-dependent Preisach models to investigate the limitations of modelling isothermal remanent magnetization acquisition curves with cumulative log Gaussian functions. *Geophysical Journal International*, *157*(1), 55–63. https://doi.org/10.1111/j.1365-246X.2004.02155.x

Ho, K., & Chen, J. (1996). Geochemistry and origin of tektites from the Penglei area, Hainan Province, southern China. *Journal of Southeast Asian Earth Sciences*, *13*(1), 61–72. https://doi.org/10.1016/0743-9547(96)00005-0

Hood, L. L., & Artemieva, N. A. (2008). Antipodal effects of lunar basin-forming impacts: Initial 3D simulations and comparisons with observations. *Icarus*, *193*(2), 485–502. https://doi.org/10.1016/j.icarus.2007.08.023

Hou, Y. M., Potts, R., Yuan, B. Y., Guo, Z. T., Deino, A., Wang, W., et al. (2000). Mid-Pleistocene Acheulean-like stone technology of the Bose basin, South China. *Science*, *287*(5458), 1622–1626. https://doi.org/10.1126/science.287.5458.1622

Howard, K. T. (2011). Volatile enhanced dispersal of high velocity impact melts and the origin of tektites. *Proceedings of the Geologists' Association*, *122*(3), 363–382. https://doi.org/10.1016/j.pgeola.2010.11.006

Hyodo, M., Matsu'ura, S., Kamishima, Y., Kondo, M., Takeshita, Y., Kitaba, I., et al. (2011). High-resolution record of the Matuyama-Brunhes transition constrains the age of Javanese Homo erectus in the Sangiran dome, Indonesia. *Proceedings of the National Academy of Sciences of the United States of America*, *108*(49), 19563–19568. https://doi.org/10.1073/pnas.1113106108

Johnson, H. P., Lowrie, W., & Kent, D. V. (1975). Stability of anhysteretic remanent magnetization in fine and coarse magnetite and maghemite particles. *Geophysical Journal of the Royal Astronomical Society*, *41*, 1–10. https://doi.org/10.1111/j.1365-246X.1975.tb05480.x

Jones, E. M., & John, W. K. (1982). Atmospheric effects of large body impacts: The first few minutes. *Geological Society of America Special Paper*, *190*, 175–186. https://doi.org/10.1130/spe190-p175

Jourdan, F., Nomade, S., Wingate, M. T. D., Eroglu, E., & Deino, A. (2019). Ultraprecise age and formation temperature of the Australasian tektites constrained by $^{40}Ar/^{39}Ar$ analyses. *Meteoritics & Planetary Sciences*, *54*(10), 2573–2591. https://doi.org/10.1111/maps.13305

Kars, M., Aubourg, C., & Pozzi, J. P. (2011). Low temperature magnetic behaviour near 35 K in unmetamorphosed claystones. *Geophysical Journal International*, *186*(3), 1029–1035. https://doi.org/10.1111/j.1365-246X.2011.05121.x

Kenkmann, T., Maier, R. V., Sturm, S., & Zhu, M. H. (2014). A new tektite discovery in the Guangdong Province, China, and the search for the source crater of the Australasian tektites. In *The seventy-seventh annual meteoritical society meeting*. (p. 5322).

King, J. W., Banerjee, S. K., & Marvin, J. (1983). A new rock-magnetic approach to selecting sediments for geomagnetic paleointensity studies Application to paleointensity for the last 4000 years. *Journal of Geophysical Research*, *88*(B7), 5911–5921. https://doi.org/10.1029/JB088iB07p05911

Kirova, O. A. (1964). Scattered matter from the area of fall of the Tunguska cometary meteorite. *Annals of the New York Academy of Sciences*, *119*(1), 235–242. https://doi.org/10.1111/j.1749-6632.1965.tb47436.x

Klein, L. C., Yinnon, H., & Uhlmann, D. R. (1980). Viscous flow and crystallization behavior of tektite glass. *Journal of Geophysical Research*, *85*(B10), 5485–5489. https://doi.org/10.1029/JB085iB10p05485

Kleinmann, B. (1969). Magnetite bearing spherules in tektites. *Geochimica et Cosmochimica Acta*, *33*(9), 1113–1120. https://doi.org/10.1016/0016-7037(69)90067-2

Koeberl, C. (1986). Geochemistry of tektites and impact glasses. *Annual Review of Earth and Planetary Sciences*, *14*(1), 323–350. https://doi.org/10.1146/annurev.ea.14.050186.001543

Koeberl, C. (1992). Geochemistry and origin of Muong Nong-type tektites. *Geochimica et Cosmochimica Acta*, *56*(3), 1033–1064. https://doi.org/10.1016/0016-7037(92)90046-L

Koeberl, C. (1994). Tektite origin by hypervelocity asteroidal or cometary impact: Target rocks, source craters, and mechanisms. *Geological Society of America Special Paper*, *293*, 133–151. https://doi.org/10.1130/spe293-p133

Koeberl, C., Bottomley, R., Glass, B. P., & Storzer, D. (1997). Geochemistry and age of Ivory Coast tektites and microtektites. *Geochimica et Cosmochimica Acta*, *61*(8), 1745–1772. https://doi.org/10.1016/S0016-7037(97)00026-4

Koeberl, C., Glass, B. P., Schulz, T., Wegner, W., Giuli, G., Cicconi, M. R., et al. (2022). Tektite glasses from Belize, Central America: Petrography, geochemistry, and search for a possible meteoritic component. *Geochimica et Cosmochimica Acta*, *325*, 232–257. https://doi.org/10.1016/j.gca.2022.02.021

Kohout, T., Kosterov, A., Haloda, J., Týcová, P., & Zbořil, R. (2010). Low-temperature magnetic properties of iron-bearing sulfides and their contribution to magnetism of cometary bodies. *Icarus*, *208*(2), 955–962. https://doi.org/10.1016/j.icarus.2010.03.021

Kohout, T., Kosterov, A., Jackson, M., Pesonen, L. J., Kletetschka, G., & Lehtinen, M. (2007). Low-temperature magnetic properties of the Neuschwanstein EL6 meteorite. *Earth and Planetary Science Letters*, *261*(1–2), 143–151. https://doi.org/10.1016/j.epsl.2007.06.022

Kosterov, A. (2001). Magnetic hysteresis of pseudo-single-domain and multidomain magnetite below the Verwey transition. *Earth and Planetary Science Letters*, *186*(2), 245–253. https://doi.org/10.1016/S0012-821X(01)00250-3

Krizova, S., Skala, R., Halodova, P., Zak, K., & Ackerman, L. (2019). Near end-member shenzhuangite, $NiFeS_2$, found in Muong Nong-type tektites from Laos. *American Mineralogist*, *104*(8), 1165–1172. https://doi.org/10.2138/am-2019-6930

Lagroix, F., & Guyodo, Y. (2017). A new tool for separating the magnetic mineralogy of complex mineral assemblages from low temperature magnetic behavior. *Frontiers of Earth Science*, *5*, 61. https://doi.org/10.3389/feart.2017.00061

Lanci, L., & Kent, D. V. (2006). Meteoric smoke fallout revealed by superparamagnetism in Greenland ice. *Geophysical Research Letters*, *33*(13), L13308. https://doi.org/10.1029/2006GL026480

Lanci, L., Kent, D. V., Biscaye, P. E., & Bory, A. (2001). Isothermal remanent magnetization of Greenland ice Preliminary result. *Geophysical Research Letters*, *28*(8), 1639–1642. https://doi.org/10.1029/2000GL012594

Lee, M. Y., & Wei, K. Y. (2000). Australasian microtektites in the South China Sea and the west Philippine Sea: Implications for age, size, and location of the impact crater. *Meteoritics & Planetary Sciences*, *35*(6), 1151–1155. https://doi.org/10.1111/j.1945-5100.2000.tb01504.x

Lee, Y., Chen, J., Ho, K., & Juang, W. S. (2004). Geochemical studies of tektites from East Asia. *Geochemical Journal*, *38*, 1–17. https://doi.org/10.2343/geochemj.38.1

Li, D. M. (1963). A preliminary survey and study of the tektites: Lei-Gong-Mo–from Leichow peninsula and Hainan island, China. *Scientia Geologica Sinica*, *1*, 42–49. (in Chinese with English abstract).

Li, H., Lotter, M. G., Kuman, K., Lei, L., & Wang, W. (2021). Population dynamics during the Acheulean at ∼0.8 Ma in East and Southeast Asia: Considering the influence of two geological cataclysms. *Palaeogeography, Palaeoclimatology, Palaeoecology*, *562*, 109927. https://doi.org/10.1016/j.palaeo.2020.109927

Lin, S., Guan, Y. B., & Hsu, W. B. (2011). Geochemistry and origin of tektites from Guilin of Guangxi, Guangdong and Hainan. *Science China Earth Sciences*, *54*(3), 349–358. https://doi.org/10.1007/s11430-010-4146-1

Louzada, K. L., Weiss, B. P., Maloof, A. C., Stewart, S. T., Swanson-Hysell, N. L., & Soule, S. A. (2008). Paleomagnetism of Lonar impact crater, India. *Earth and Planetary Science Letters*, *275*(3–4), 308–319. https://doi.org/10.1016/j.epsl.2008.08.025

Ma, P., Aggrey, K., Tonzola, C., Schnabel, C., de Nicola, P., Herzog, G. F., et al. (2004). Beryllium-10 in Australasian tektites: Constraints on the location of the source crater. *Geochimica et Cosmochimica Acta*, *68*(19), 3883–3896. https://doi.org/10.1016/j.gca.2004.03.026

Ma, Q., Zheng, J. P., Griffin, W. L., Zhang, M., Tang, H. Y., Su, Y. P., & Ping, X. (2012). Triassic "adakitic" rocks in an extensional setting (North China): Melts from the cratonic lower crust. *Lithos*, *149*, 159–173. https://doi.org/10.1016/j.lithos.2012.04.017

Macris, C. A., Asimow, P. D., Badro, J., Eiler, J. M., Zhang, Y., & Stolper, E. M. (2018). Seconds after impact: Insights into the thermal history of impact ejecta from diffusion between lechatelierite and host glass in tektites and experiments. *Geochimica et Cosmochimica Acta*, *241*, 69–94. https://doi.org/10.1016/j.gca.2018.08.031

Magna, T., Deutsch, A., Mezger, K., Skala, R., Seitz, H. M., Mizera, J., et al. (2011). Lithium in tektites and impact glasses: Implications for sources, histories and large impacts. *Geochimica et Cosmochimica Acta*, *75*(8), 2137–2158. https://doi.org/10.1016/j.gca.2011.01.032

Maher, B. A. (1988). Magnetic properties of some synthetic sub-micron magnetites. *Geophysical Journal*, *94*(1), 83–96. https://doi.org/10.1111/j.1365-246X.1988.tb03429.x

Maxbauer, D. P., Feinberg, J. M., & Fox, D. L. (2016). MAX UnMix: A web application for unmixing magnetic coercivity distributions. *Computers & Geosciences*, *95*, 140–145. https://doi.org/10.1016/j.cageo.2016.07.009

Melosh, H. J. (1990). Vapor plumes: A neglected aspect of impact cratering. *Meteoritics*, *25*, 386.

Melosh, H. J. (2020). The Australasian tektite source crater: Found at last. *Proceedings of the National Academy of Sciences of the United States of America*, *117*(3), 1252–1253. https://doi.org/10.1073/pnas.1920576117

Mizera, J. (2022). Quest for the Australasian impact crater: Failings of the candidate location at the Bolaven Plateau, Southern Laos. *Meteoritics & Planetary Sciences*, *57*(11), 1–14. https://doi.org/10.1111/maps.13912

Mizera, J., Řanda, Z., & Kameník, J. (2016). On a possible parent crater for Australasian tektites: Geochemical, isotopic, geographical and other constraints. *Earth-Science Reviews*, *154*, 123–137. https://doi.org/10.1016/j.earscirev.2015.12.004

Moskowitz, B. M., Frankel, R. B., Bazylinski, D. A., Jannasch, H. W., & Lovley, D. R. (1989). A comparison of magnetite particles produced anaerobically by magnetotactic and dissimilatory iron-reducing bacteria. *Geophysical Research Letters*, *16*(7), 665–668. https://doi.org/10.1029/GL016i007p00665

Nayak, M. T., Desa, J. A. E., & Babu, P. D. (2018). Magnetic and spectroscopic studies of an iron lithium calcium silicate glass and ceramic. *Journal of Non-Crystalline Solids*, *484*, 1–7. https://doi.org/10.1016/j.jnoncrysol.2017.12.050

Nichiporuk, W., & Chodos, A. A. (1959). The concentration of vanadium, chromium, iron, cobalt, nickel, copper, zinc, and arsenic in the meteoritic iron sulfide nodules. *Journal of Geophysical Research*, *64*(12), 2451–2463. https://doi.org/10.1029/jz064i012p02451

Nininger, H. H., & Huss, G. I. (1967). Tektites that were partially plastic after completion of surface sculpturing. *Science*, *157*(3784), 61–62. https://doi.org/10.1126/science.157.3784.61

Olsen, E. J., Kracher, A., Davis, A. M., Steele, I. M., Hutcheon, D. I., & Bunch, T. E. (1999). The phosphates of IIIAB iron meteorites. *Meteoritics & Planetary Sciences*, *34*(2), 285–300. https://doi.org/10.1111/j.1945-5100.1999.tb01752.x

Ostertag, W., Erickson, A. A., & Williams, J. P. (1969). Magnetic susceptibility of some synthetic and natural tektites. *Journal of Geophysical Research*, *74*(27), 6805–6810. https://doi.org/10.1029/JB074i027p06805

Paterson, G. A., Zhao, X., Jackson, M., & Heslop, D. (2018). Measuring, processing, and analyzing hysteresis data. *Geochemistry, Geophysics, Geosystems*, *19*(7), 1925–1945. https://doi.org/10.1029/2018GC007620

Philpotts, J. A., & Pinson, W. H. (1966). New data on the chemical composition and origin of moldavites. *Geochimica et Cosmochimica Acta*, *30*(3), 253–266. https://doi.org/10.1016/0016-7037(66)90001-9

Pike, C. R., Roberts, A. P., & Verosub, K. L. (2001). First-order reversal curve diagrams and thermal relaxation effects in magnetic particles. *Geophysical Journal International*, *145*(3), 721–730. https://doi.org/10.1046/j.0956-540x.2001.01419.x

Prasad, M. S., Mahale, V. P., & Kodagali, V. N. (2007). New sites of Australasian microtektites in the central Indian Ocean: Implications for the location and size of source crater. *Journal of Geophysical Research*, *112*(E6), E06007. https://doi.org/10.1029/2006JE002857

Reid, A. M., Park, F. R., & Cohen, A. J. (1964). Synthetic metallic spherules in a Philippine tektite. *Geochimica et Cosmochimica Acta*, *28*(6), 1009–1010. https://doi.org/10.1016/0016-7037(64)90048-1

Roberts, A. P., Cui, Y., & Verosub, K. L. (1995). Wasp-waisted hysteresis loops: Mineral magnetic characteristics and discrimination of components in mixed magnetic systems. *Journal of Geophysical Research*, *100*(B9), 17909–17924. https://doi.org/10.1029/95JB00672

Roberts, A. P., Pike, C. R., & Verosub, K. L. (2000). First-order reversal curve diagrams: A new tool for characterizing the magnetic properties of natural samples. *Journal of Geophysical Research*, *105*(B12), 28461–28475. https://doi.org/10.1029/2000JB900326

Roberts, A. P., Tauxe, L., Heslop, D., Zhao, X., & Jiang, Z. X. (2018). A critical appraisal of the "Day" diagram. *Journal of Geophysical Research: Solid Earth*, *123*(4), 2618–2644. https://doi.org/10.1002/2017JB015247

Rochette, P., Beck, P., Bizzarro, M., Braucher, R., Cornec, J., Debaille, V., et al. (2021). Impact glasses from Belize represent tektites from the Pleistocene Pantasma impact crater in Nicaragua. *Communications Earth & Environment*, *2*(1), 94. https://doi.org/10.1038/s43247-021-00155-1

Rochette, P., Bezaeva, N. S., Beck, P., Debaille, V., Folco, L., Gattacceca, J., et al. (2022). Obsidian and mafic volcanic glasses from the Philippines and Vietnam found in the Paris Museum Australasian tektite collection. *Meteoritics & Planetary Sciences*, *57*(7), 1–12. https://doi.org/10.1111/maps.13825

Rochette, P., Bezaeva, N. S., Kosterov, A., Gattacceca, J., Masaitis, V. L., Badyukov, D. D., et al. (2019). Magnetic properties and redox state of impact glasses: A review and new case studies from Siberia. *Geosciences*, *9*(5), 225. https://doi.org/10.3390/geosciences9050225

Rochette, P., Braucher, R., Folco, L., Horng, C. S., Aumaître, G., Bourlès, D. L., & Keddadouche, K. (2018). ^{10}Be in Australasian microtektites compared to tektites: Size and geographic controls. *Geology*, *46*(9), 803–806. https://doi.org/10.1130/G45038.1

Rochette, P., Fillion, G., Mittei, J., & Dekkers, M. J. (1990). Magnetic transition at 30-34 Kelvin in pyrrhotite; insight into a widespread occurrence of this mineral in rocks. *Earth and Planetary Science Letters*, *98*(3–4), 319–328. https://doi.org/10.1016/0012-821X(90)90034-U

Rochette, P., Gattacceca, J., Devouard, B., Moustard, F., Bezaeva, N. S., Cournède, C., & Scaillet, B. (2015). Magnetic properties of tektites and other related impact glasses. *Earth and Planetary Science Letters*, *432*, 381–390. https://doi.org/10.1016/j.epsl.2015.10.030

Schlinger, C. M., Rosenbaum, J. G., & Veblen, D. R. (1988). Fe-oxide microcrystals in welded tuff from southern Nevada; origin of remanence carriers by precipitation in volcanic glass. *Geology*, *16*(6), 556–559. https://doi.org/10.1130/0091-7613(1988)016<0556:FOMIWT>2.3.CO;2

Schlinger, C. M., & Smith, R. M. (1986). Superparamagnetism in volcanic glasses of the KBS Tuff: Transmission electron microscopy and magnetic behavior. *Geophysical Research Letters*, *13*(8), 729–732. https://doi.org/10.1029/GL013i008p00729

Schnetzler, C. C., Walter, L. S., & Marsh, J. G. (1988). Source of the Australasian tektite strewn field A possible offshore impact site. *Geophysical Research Letters*, *15*(4), 357–360. https://doi.org/10.1029/gl015i004p00357

Schreiber, H. D., Minnix, L. M., Balazs, G. B., Pye, L. D., O'Keefe, J. A., & Frechette, V. D. (1984). The redox state of iron in tektites. *Journal of Non-Crystalline Solids*, *67*(1–3), 349–359. https://doi.org/10.1016/0022-3093(84)90160-1

Schwarcz, H. P. (1962). A possible origin of tektites by soil fusion at impact sites. *Nature*, *194*(4823), 8–10. https://doi.org/10.1038/194008a0

Senftle, F. E., & Thorpe, A. (1959). Magnetic susceptibility of tektites and some other glasses. *Geochimica et Cosmochimica Acta*, *17*(3–4), 234–247. https://doi.org/10.1016/0016-7037(59)90098-5

Senftle, F. E., Thorpe, A. N., Grant, J. R., Hildebrand, A., Moholy-Nagy, H., Evans, B. J., & May, L. (2000). Magnetic measurements of glass from Tikal, Guatemala: Possible tektites. *Journal of Geophysical Research*, *105*(B8), 18921–18925. https://doi.org/10.1029/2000jb900125

Senftle, F. E., Thorpe, A. N., & Lewis, R. R. (1964). Magnetic properties of nickel-iron spherules in tektites from Isabela, Philippine Islands. *Journal of Geophysical Research*, *69*(2), 317–324. https://doi.org/10.1029/JZ069i002p00317

Sieh, K., Herrin, J., Jicha, B., Schonwalder Angel, D., Moore, J. D. P., Banerjee, P., et al. (2020). Australasian impact crater buried under the Bolaven volcanic field, Southern Laos. *Proceedings of the National Academy of Sciences of the United States of America*, *117*(3), 1346–1353. https://doi.org/10.1073/pnas.1904368116

Smirnov, A. V., & Tarduno, J. A. (2011). Development of a low-temperature insert for the measurement of remanent. *Geochemistry, Geophysics, Geosystems*, *12*(4), Q04Z23. https://doi.org/10.1029/2011GC003517

Spaepen, F., & Turnbull, D. (1984). Metallic glasses. *Annual Review of Physical Chemistry*, *35*(1), 241–263. https://doi.org/10.1146/annurev.pc.35.100184.001325

Stähle, V. (1972). Impact glasses from the suevite of the Nördlinger Ries. *Earth and Planetary Science Letters*, *17*(1), 275–293. https://doi.org/10.1016/0012-821X(72)90287-7

Starunov, V. A., Kosterov, A., Sergienko, E. S., Yanson, S. Y., Markov, G. P., Kharitonskii, P. V., et al. (2019). Magnetic properties of tektite-like impact glasses from Zhamanshin astrobleme, Kazakhstan. In D. Nurgaliev (Ed.), *Recent advances in rock magnetism, environmental magnetism and paleomagnetism* (1nd ed., pp. 445–465). Springer Geophysics. https://doi.org/10.1007/978-3-319-90437-5_30

Stöffler, D., Artemieva, N. A., & Pierazzo, E. (2002). Modeling the Ries-Steinheim impact event and the formation of the moldavite strewn field. *Meteoritics & Planetary Sciences*, *37*(12), 1893–1907. https://doi.org/10.1111/J.1945-5100.2002.TB01171.X

Tada, T., Tada, R., Chansom, P., Songtham, W., Carling, P. A., & Tajika, E. (2020). In situ occurrence of Muong Nong-type Australasian tektite fragments from the Quaternary deposits near Huai Om, northeastern Thailand. *Progress in Earth and Planetary Science*, *7*(1), 66. https://doi.org/10.1186/s40645-020-00378-4

Tauxe, L. (1993). Sedimentary records of relative paleointensity of the geomagnetic field: Theory and practice. *Reviews of Geophysics*, *31*(3), 319–354. https://doi.org/10.1029/93RG01771

Taylor, S. R. (1962). Fusion of soil during meteorite impact, and the chemical composition of tektites. *Nature*, *195*(4836), 32–33. https://doi.org/10.1038/195032a0

Thorpe, A. N., & Senftle, F. E. (1964). Submicroscopic spherules and color of tektites. *G Geochimica et Cosmochimica Acta*, *28*(6), 981–994. https://doi.org/10.1016/0016-7037(64)90045-6

Thorpe, A. N., Senftle, F. E., & Cuttitta, F. (1963). Magnetic and chemical investigations of iron in tektites. *Nature*, *197*(4870), 836–840. https://doi.org/10.1038/197836a0

von Engelhardt, W., Berthold, C., Wenzel, T., & Dehner, T. (2005). Chemistry, small-scale inhomogeneity, and formation of moldavites as condensates from sands vaporized by the Ries impact. *Geochimica et Cosmochimica Acta*, *69*(23), 5611–5626. https://doi.org/10.1016/j.gca.2005.07.004

Wasilewski, P. J., & Dickinson, T. (2000). Aspects of the validation of magnetic remanence in meteorites. *Meteoritics & Planetary Sciences*, *35*(3), 537–544. https://doi.org/10.1111/j.1945-5100.2000.tb01434.x

Weiss, B. P., Pedersen, S., Garrick-Bethell, I., Stewart, S. T., Louzada, K. L., Maloof, A. C., & Swanson-Hysell, N. L. (2010). Paleomagnetism of impact spherules from Lonar crater, India and a test for impact-generated fields. *Earth and Planetary Science Letters*, *298*(1–2), 66–76. https://doi.org/10.1016/j.epsl.2010.07.028

Werner, T., & Borradaile, G. J. (1998). Homogeneous magnetic susceptibilities of tektites: Implications for extreme homogenization of source material. *Physics of the Earth and Planetary Interiors*, *108*(3), 235–243. https://doi.org/10.1016/S0031-9201(98)00098-3

Westgate, J. A., Pillans, B. J., Alloway, B. V., Pearce, N. J. G., & Simmonds, P. (2021). New fission-track ages of Australasian tektites define two age groups: Discriminating between formation and reset ages. *Quaternary Geochronology*, *66*, 101113. https://doi.org/10.1016/j.quageo.2020.101113

Whymark, A. (2018). Further geophysical data in the search for the Australasian tektite source crater location in the Song Hong-Yinggehai Basin, Gulf of Tonkin. In *Proceeding of the forty-ninth lunar and planetary science conference* (Vol. 1078).

Whymark, A. (2021). A review of evidence for a Gulf of Tonkin location for the Australasian tektite source crater. *Thai Geoscience Journal*, *2*(2), 1–29. https://doi.org/10.14456/tgj.2021.2

Wilding, M., Webb, S., & Dingwell, D. B. (1996). Tektite cooling rates: Calorimetric relaxation geospeedometry applied to a natural glass. *Geochimica et Cosmochimica Acta*, *60*(6), 1099–1103. https://doi.org/10.1016/0016-7037(96)00010-5

Yan, P., Xiao, Z. Y., Xiao, G. Q., Pan, Q., Hui, H. J., Wu, Y. H., et al. (2022). Undetection of Australasian microtektites in the Chinese Loess Plateau. *Palaeogeography, Palaeoclimatology, Palaeoecology*, *585*, 110721. https://doi.org/10.1016/j.palaeo.2021.110721

Yan, Z., Yuan, B. Y., & Ye, L. F. (1979). Fission track ages of Lei Gong Mo from Hainan Island. *Scientia Geologica Sinica*, *1*, 37–42. (in Chinese with English abstract).

Yu, Y. J., Dunlop, D. J., & Ozdemir, O. (2002). Partial anhysteretic remanent magnetization in magnetite 1. Additivity. *Journal of Geophysical Research*, *107*(B10), EPM7-1–EPM7-9. https://doi.org/10.1029/2001JB001249

Yuan, B. Y. (1981). Preliminary discussion on the origin of Lei-Gong-Mo (tektites). *Scientia Geologica Sinica*, *16*(4), 329–336. (in Chinese with English abstract).

Zhang, H. N., Chen, W. G., Li, Z. Q., Zhang, F. L., & Yuan, B. Y. (1991). Discovery of tektite in west Guangdong and its sense for determination of the age. *Marine Geology & Quaternary Geology*, *11*(4), 101–108. (in Chinese with English abstract). https://doi.org/10.16562/j.cnki.0256-1492.1991.04.012

Zhu, Z. Y., Xie, J. B., Zheng, Y. Q., Mo, S., Yang, C., Rao, Z. G., et al. (2006). Neotectonics along the north coast of South China Sea and its regional correlation around the boundary of the Early and Middle Pleistocene. *Quaternary Sciences*, *26*(1), 70–76. (in Chinese with English abstract). https://doi.org/10.3321/j.issn:1001-7410.2006.01.009

Zhu, Z. Y., Zhou, H. Y., Qiao, Y. L., Zhang, H. X., & Liang, J. P. (2001). Initial strata occurrence of the South China tektites in strata and its implication for event-stratigraphy. *Journal of Geomechanics*, *7*(4), 296–302. (in Chinese with English abstract). https://doi.org/10.3969/j.issn.1006-6616.2001.04.002

References From the Supporting Information

Roberts, A. P., Heslop, S., Zhao, X., & Pike, C. R. (2014). Understanding fine magnetic particle systems through use of first-order reversal. *Reviews of Geophysics*, *52*(4), 557–602. https://doi.org/10.1002/2014RG000462

Robertson, D. J., & France, D. E. (1994). Discrimination of remanence-carrying minerals in mixtures, using isothermal remanent magnetization acquisition curves. *Physics of the Earth and Planetary Interiors*, *82*(3–4), 223–234. https://doi.org/10.1016/0031-9201(94)90074-4

Stine, J., Geissman, J. W., Sweet, D. E., & Baird, H. (2021). The effect of differential weathering on the magnetic properties of paleosols: A case study of magnetic enhancement vs. magnetic depletion in the Pleistocene Blackwater draw formation, Texas. *Frontiers of Earth Science*, *9*, 601401. https://doi.org/10.3389/feart.2021.601401